AI-3000K Infrared Line List for Hot CO_2

Xinchuan Huang(黄新川),[1a,b] Richard S. Freedman,[2a,b] Sergey Tashkun,[3c]
David W. Schwenke,[4d] and Timothy J. Lee[5e]

[a] MS 245-6, Astrophysics Branch, Space Science and Astrobiology Division, NASA Ames Research Center, Moffett Field, CA 94035, USA

[b] SETI Institute, 339 Bernardo Avenue, Suite 200, Mountain View, CA 94043, USA

[c] Laboratory of Theoretical Spectroscopy, V.E. Zuev Institute of Atmospheric Optics, Russian Academy of Sciences, Academician Zuev square 1, Tomsk 634055, Russia

[d] MS 258-2, NAS Facility, NAS Ames Research Center, Moffett Field, CA 94035, USA

[e] MS 245-3, Planetary Systems Branch, Space Science and Astrobiology Division, NASA Ames Research Center, Moffett Field, CA 94035, USA

Submit to Journal of Molecular Spectroscopy

[1] Corresponding Author: Xinchuan.Huang-1@nasa.gov
[2] Email: Richard.S.Freedman@nasa.gov
[3] Email: tashkun@iao.ru
[4] Email: David.W.Schwenke@nasa.gov
[5] Email: Timothy.J.Lee@nasa.gov

Abstract

AI-3000K is a semi-empirical IR line list constructed for hot CO_2 spectra analysis and simulation up to 3000 – 4000 K. Compared to previously published Ames-1000K and UCL-4000, it represents a major upgrade, utilizing a new algorithm for optimization and including the latest improvements in potential energy surface (PES), dipole moment surface (DMS), and room temperature IR line list (Ames-2021 296K). To maximize the success of introducing experimental based accurate line positions, a new PES (X01d) was refined with respect to more than 800 selected CDSD2019 [Tashkun et al. JQSRT (2019) **228**, 124] energy levels in the range of 0 – 24,000 cm^{-1}, with σ_{rms} = 0.5 – 0.7 cm^{-1}. Most differences between the X01d PES based levels and CDSD2019 energies are within ±2 cm^{-1}. A new DMS is fitted from extrapolated CCSD(T)/aug-cc-pV(T,Q,5)Z dipole calculations, with $\sigma_{rms} = 5.1 \times 10^{-6}$ au for 11155 geometries up to 40000 cm^{-1}, denoted Ames-2021-40K. Compared to the best available Ames-2021 DMS and room temperature IR line list [Huang et al J. Phys. Chem. A (2022) **126**, 5940], the relative intensity differences are expected to be ~1‰. The line position accuracy of "X01d + Ames-2021-40K" IR line list is significantly improved by adopting CDSD2019 energy levels up to 24000 cm^{-1} ($J \leq 150$). The Einstein A_{21} coefficients for E'<15000 cm^{-1} transitions are replaced by more accurate values from the Ames-2021 296K IR line list. In short, the AI-3000K is the X01d PES and Ames-2021-40K DMS based line list enhanced with the A_{21} of Ames-2021 296K line list and CDSD energy levels. It provides continuous coverage from 0 to 20000 cm^{-1} for the four most abundant isotopologues: $^{12}C^{16}O_2$ (626), $^{13}C^{16}O_2$ (636), $^{16}O^{12}C^{18}O$ (628), and $^{16}O^{12}C^{17}O$ (627). The impacts of isotopologue and E'/E'' cutoffs have been examined. Intensity convergence (not accuracy) of AI-3000K line list is quantitatively estimated in 1 cm^{-1} bins. It is better than 99% in the whole range of 0 – 20000 (10000) cm^{-1} at 1000 K (2000 K), or better than 90% in the whole range of 0 – 15000 (9000) cm^{-1} at 2000 K (3000 K), respectively. Convergence beyond 3000 K will require a new PES and DMS for E' > 40000 cm^{-1}. The AI-3000K and HITEMP based IR simulations are compared to high resolution shock tube experiments for CO_2-Ar mixture up to 2000 K. With line position accuracy comparable to that of HITEMP, AI-3000K IR line list yields better agreements at more frequencies. Potential sources of discrepancies with experiment are discussed.

I. Introduction

Carbon Dioxide, CO_2, is the second most important greenhouse gas (water is primary) on the Earth [1] and involved in industrial and combustion processes. It also widely exists in Solar system planets [2–7], moons [8–12], comets [13,14], as well as dwarfs [15,16], and extrasolar planetary atmospheres [17–22]. CO_2 remote sensing is critical for Venus/Earth/Mars-like exoplanet studies [3,23]. The line-by-line spectroscopic analysis for Venus atmospheres can be traced back to 1990's [24], where CO_2 constitutes 95% of the Venus atmosphere. CO_2 is expected to play important roles in directly imaged exoplanets [25], from lower mass exoplanets [26] to hot large exoplanets where the main constituents of the atmospheres are likely to be very stable molecules such as H_2O, CO, CO_2, NH_3, etc. Therefore, a reliable hot CO_2 opacity database for a wide spectral range and a wide temperature range may serve as a powerful chemical diagnostic tool for their atmosphere environment and physical conditions, e.g., temperature, pressure, and density. It will greatly facilitate or enhance the accuracy of opacity modeling in hot exoplanetary studies and spectral data analysis utilizing the astronomical data from ground, air, or space-based observatories, including ongoing JWST [27,28] and future ARIEL [29], NGRST [30] and LUVOIR [31]. Examples in planetary atmosphere studies can be found in Refs. [2,16,18,32–36].

In last 20 years, important progresses have been made on CO_2 IR line lists for room temperature analysis [37–46], as well as those lists targeting higher temperature applications [38,43,47–53]. Compared to the Direct Numerical Diagonalization (DND) approach [54,55] based High-T database [47,48,56] utilized in 1993 Venus study [24], the current Carbon Dioxide Spectroscopic Databank (CDSD) line list series [39,45,49,50] utilizes global Effective Hamiltonian [57] models and Effective Dipole Moment (EDM) [58,59] models fitted from high-resolution experimental data, while the line position and intensity of Ames [37,38,43,52] and UCL [40–42] IR line lists are variationally computed using semi-empirically refined *ab initio* potential energy surface (PES) and high quality *ab initio* dipole moment surface (DMS). Recent HITRAN updates [44,46], UCL-4000 [53], and Ames-2021 [60] also have tried to combine the advantages of experimental data and quantum rovibrational calculations. However, there are still many deficiencies and missing data in higher energy ranges, or for weaker bands. These inaccuracies may become significant at high temperature and cause difficulties in IR analysis or generate noticeable modeling deviations.

In this paper we report a new IR line list for hot CO_2 studies, denoted AI-3000K. It includes $J \leq 250$, $E' \leq 40{,}000$ cm^{-1} transitions for $^{12}C^{16}O_2$, and $J \leq 200$, $E' \leq 36{,}000$ cm^{-1} transitions for $^{13}C^{16}O_2$, $^{16}O^{12}C^{18}O$, and $^{16}O^{12}C^{17}O$. Convergence analysis suggests the AI-3000K intensity is more than 90%+ converged in the whole range from 0 to 16,000 cm^{-1} at 2000 K, or from 0 to 9000 cm^{-1} at 3000 K. It takes advantages of the accurate CDSD energy levels up to 24,000 cm^{-1} and more reliable line intensities computed for the strong transitions between energy levels up to 15,000 cm^{-1}, using best available PES [37,43] and DMS [60]. We expect it will facilitate future hot CO_2 IR analysis and simulations. The line list name is abbreviated from 'Ames' for line list calculations and 'IAO' for CDSD energy, respectively.

This paper is organized as following. Section 2 gives a review of the published hot CO_2 IR line lists; Section 3 introduces the necessity and details of a CDSD based PES refinement, the DMS choice, and the generation procedure and storage of the AI-3000K line list; Section 4 presents three types of convergence analysis for the line list, and Section 5 compares our new results to published line lists and shock-tube high-resolution experiment near 2000 K; Section 6 summarizes the known progresses and potential deficiencies, and discusses future upgrades.

II. Published Hot CO_2 IR Line Lists

II.1 High-T

Wattson's High-T list [47,48,56] for CO_2 was computed variationally on PES and DMS which were completely empirical, with all parameters determined by matching to experimental data. In the range of 500 – 12,500 cm^{-1}, it includes ~60,000 bands and 7.2 million lines that are stronger than 10^{-30} cm^{-1}/molecule.cm^{-2} at 750K. Compared to earlier HITRAN versions (86' and 91'), it represented a remarkable leap in both wavenumber coverage and vibrational band completeness. It had excellent interpolation consistency and reasonable intensity for bands with strong or medium intensities from room temperature to 750K. Uncertainty estimate was 10-20% for intensity and 0.01~0.1 cm^{-1} for line positions.

Such quality and improvement were due to the availability of extensive experimental data. However since the parameters are empirical, this also sets a ceiling for its extrapolation or prediction reliability. For example, then-existing experimental data did not contain sufficient information to determine some higher-order dipole terms that may play important roles for the intensity of certain weak bands and high energy bands. Consequently, the intensity in several trough regions below 5000 cm^{-1} was overestimated by 1~2 orders of magnitude, from 10^{-23} cm^{-1}/molecule.cm^{-2} at 1500K to 10^{-22} cm^{-1}/molecule.cm^{-2} at 3000K. See examples in Fig.6 of Ref. [52] and Fig.16a of Ref. [43].

II.2 CDSD-1000, 4000, and HITEMP2010

The CDSD-1000 databank [49] contains the line parameters (positions, intensities, air- and self-broadened half-widths and coefficients of temperature dependence of air-broadened half-widths) of the four most abundant isotopic species. The reference temperature is 1000 K and the intensity cutoff is 10^{-27} cm^{-1}/molecule.cm^{-2}. The databank has been generated within the framework of the method of effective operators and based on the global fitting of spectroscopic parameters (parameters of the effective Hamiltonians and effective dipole moment operators) to observed data collected from the literature. A semi-empirical model was used for calculations of line widths. The databank has more than 3 million entries covering the 263–9648 cm^{-1} spectral range.

The CDSD-4000 databank [50] is based on the same principles as CDSD-1000. The reference temperature is 296K and the intensity cutoff is 10^{-27} cm^{-1}/molecule.cm^{-2} at 4000K. The databank has more than 628 million entries, covers the 226–8310 cm^{-1} spectral range and was designed for the temperature range 2500–5000K. The maximum value of the rotational quantum number J is 300 and the energy cutoff values is 44,000 cm^{-1}. The energy cutoff is a great strength of CDSD-4000.

The $^{12}C^{16}O_2$ data in the HITEMP2010 databank [51] was taken from enlarged version of CDSD-1000 ($S_{1000K} > 10^{-27}$ cm^{-1}/molecule.cm^{-2}), CDSD-Venus ($S_{750K} > 10^{-30}$ cm^{-1}/molecule.cm^{-2}), and CDSD-296 ($S_{296K} > 10^{-30}$ cm^{-1}/molecule.cm^{-2}). It included more than 11 million lines of the 7 most abundant CO_2 isotopologues in the range of 6 – 12784 cm^{-1}, with $S_{min} = 3.5\times10^{-51}$ and $S_{max} = 3.5\times10^{-18}$ cm^{-1}/molecule.cm^{-2} at 296K.

As the effective Hamiltonian models in CDSD and HITEMP2010 [51] line lists were mostly experiment based, their line positions can be as accurate as 10^{-5}~10^{-3} cm^{-1} in the range of experimental measurements. Similar to High-T, the CDSD models also have been expanded and enhanced with new high-resolution experiments, but it is still difficult to extrapolate to very weak bands or minor isotopologues.

II.3 Ames-1000K (2013/2014)

The Ames-1000K [38,52] line lists were computed for all $^{12/13}C$ and $^{16/17/18}O$ isotopologues, with $J = 0 – 150$, $S_{296K} > 10^{-36}$ cm^{-1}/molecule.cm^{-2}, $E' < 33{,}000$ cm^{-1} for symmetric isotopologues (626, 636, 727, 737, 828, 838 and 646), $E' < 22{,}000$ cm^{-1} for asymmetric isotopologues (627,628, 637, 638, 727 and 738), and $E' < 24{,}000$ cm^{-1} for line list generations. This was the first line list to provide continuous and complete coverage from 0 to 20,000 cm^{-1}. Line shape parameters were computed for 4 temperature ranges, i.e., Mars, Earth, Venus and 700K-2000K. At 1000K, the $E' \leq 24{,}000$ cm^{-1} cutoff was adequate for the spectra range up to 18,000 cm^{-1}. At 1550K and 1773K, experimental spectra [61,62] had similar agreements with Ames-1000K and HITEMP2010 at 3500 cm^{-1} and 4900 cm^{-1}, but Ames-1000K had better agreement at 2100 cm^{-1}. Note the issue in HITEMP2010 has been solved in recent CDSD models.

For Ames-1000K and later Ames-2016 line lists, the rovibrational energy levels were variationally computed on Ames-1 [37] or Ames-2 [43] PES, and IR transition dipole moments were computed using the DMS-N2 [52] dipole surface. The Ames-1 PES was empirically refined using a few hundreds of purely experimental energy levels of $^{12}C^{16}O_2$, with $\sigma_{rms} = 0.02$ cm^{-1} for both the reference energy level set and a full experimental data set of 6873 J=0-117 levels up to 14,000 cm^{-1} [37]. A stretching basis related defect in Ames-1 PES was later fixed in Ames-2 PES [43]. Prediction accuracy primarily varies between 0.01 cm^{-1} to 0.05 cm^{-1} (e.g., below 10,000 cm^{-1}), but may also reach 0.10 ~ 0.20 cm^{-1} or larger for those states at higher energy or with higher vibrational quanta. The DMS-N2 dipole surface was determined by fitting the finite-field CCSD(T)/aug-cc-pVQZ dipole components to polynomial expansions of pseudo charges on two O nucleus, with fitting $\sigma_{rms} < 10^{-6}$ a.u. in the energy range of 0 – 30,000 cm^{-1}. For strong bands of isotopologues, the differences between the Ames 296K IR intensity predictions and recent experiments were found to be usually within ±5% [63]. Exceptions are those bands or transitions strongly impacted by Coriolis Couplings, e.g., 11101i-00001 bands at 1900 cm^{-1} [46]. An intensity gap of ~0.6% was found between the P and R branches of symmetric isotopologues, which has been fixed in recent Ames-2021 line list calculations [60] and this work.

In Ames-1000K, all lines stronger than 10^{-27} cm^{-1}/molecule.cm^{-2} or 1/1000 of the intensity sum S_{total} in each 1 cm^{-1} interval were first retained. Then the intensity cutoff was gradually reduced to incorporate weaker lines until the new intensity sum has reached at least 99.9% of S_{total}. This "99.9% in 1 cm^{-1}" screening successfully reduced the size of original Ames-1000K IR line lists by 90-95%. At the end, 650 million lines were compactly stored in 13 compressed .tgz files, occupying 18.7 GB disk space. This equals to ~16.2 bytes per line, which included upper and lower states, Einstein A_{21}, and line shape parameters at 4 temperatures. A “natural” Ames-1000K IR line list was generated from these “reduced" lists with terrestrial abundances of CO_2 isotopologues. The mixed list had 45 million lines.

II.4 Ames-4000K (2016) and UCL-4000 (2020)

Huang et al (2017) [43] reported a preliminary Ames-4000K list of $^{12}C^{16}O_2$ with $J \leq 220$, $E' < 24{,}000$ cm^{-1}, and $S_{4000K} > 10^{-30}$ cm^{-1}/molecule.cm^{-2}, using the Ames-2 PES and DMS-N2. After comparing it to several $^{12}C^{16}O_2$ subsets of CDSD-4000 line list [50] with different J and E' cutoffs, it was concluded that the $E' < 24{,}000$ cm^{-1} cutoff was the major cause of the noticeable intensity losses at 4000 K. To ensure 99.0-99.9% intensity convergence in a 1 cm^{-1} window, it is also recommended to include all lines at least 5-6 orders of magnitude weaker than the intensity sum.

Yurchenko et al (2020) [53] reported UCL-4000 IR line list for $^{12}C^{16}O_2$ in the range of 0 – 20,000 cm^{-1}, using $J \leq 202$, $E' < 36{,}000$ cm^{-1}, and $E'' < 16{,}000$ cm^{-1} cutoffs. It included 2.5 billion lines with Einstein coefficient $A_{21} > 10^{-14}$ s^{-1}. The UCL 2015 DMS [40,64] and Ames potential energy surface were adopted in their calculations. Compared to the preliminary Ames-4000K list, the $E' < 36{,}000$ cm^{-1} is a big improvement. It was expected to be valid for temperatures up to 2500 *K*. To improve the line position accuracy, all calculated rovibrational levels in a specific vibrational state were adjusted by the calc.-HITRAN difference averaged from J=0-40 residuals of the same state, or further replaced by HITRAN energies if available. Partition functions, rovibrational Obs.-Calc. errors, energy uncertainty, quantum number assignments, and 500-4000 K spectra evolutions were compared and discussed in Yurchenko et al [53]. A comparison with experiment [62] was also given at 1773 K.

Storage of UCL-4000 list followed ExoMol [65] style. It includes a list of numbered rovibrational energy levels, and a line list file containing upper and lower state #id numbers and A_{21} coefficients. The line list file was split into 20 subsets of 1000 cm^{-1} intervals. Note the data storage of Ames line lists has similar idea, but our line list files contain more information about transitions. See Section III.6 for details.

II.5 Summary

These published hot CO_2 IR line lists have taken advantages of accurate experimental data, empirically derived (or refined) PES, high quality DMS, effective Hamiltonian models, and theoretical rovibrational calculations. They were generated from either "Experiment Data based" strategy, or "Best Theory + Reliable High-resolution Experiment" (BTRHE) strategy. The Ames and UCL CO_2 line lists follow the second path, where high quality *ab initio* PES and DMS can provide quality insurance and constraints for unobserved spectra bands and minor isotopologues that have not been thoroughly studied. The main strength of this path is the completeness, reliability and consistency of the computed IR line list ***predictions*** for missing, weak or isotopologue bands, as long as they are still within the effective coverage of the PES and DMS. The major deficit is the line position accuracy, which is only as accurate as σ_{rms} = 0.01-0.02 cm^{-1} even for those bands satisfactorily refined with high resolution experimental data.

III. Technical Details: New PES, DMS, Procedure, Storage, etc.

III.1 Necessity for new PES refinement

To minimize the impact of the deficit discussed above for line position accuracy, a general trend in molecular IR line list field has been to combine the advantages of experiment and theoretical efforts. In other words, to combine the experiment-based accurate line positions and confirmed reliable intensities, with the reliable and consistent predictions for line positions and intensities. Both HITRAN2016 CO_2 list [41,42,44] and UCL-4000 [53] were good examples, where CDSD-296 [39,45] and HITRAN [44] line positions were adopted along with UCL intensities, respectively. But compared to room temperature line lists, the most challenging part at higher temperatures is to maintain a good quality control for thousands of weak bands and high lying vibrational bands, and identify and remove various numerical noises in the computed line intensities which may become significant at 1500 – 4000 K. The rovibrational energy levels in CDSD-296 [45] and HITRAN2020 [66] are for room temperature line lists, but higher temperature simply requires millions of additional levels at higher energy and higher J's. Therefore, for hot CO_2 line list, it is critical to expand the synergy between experiment based CDSD Effective

Hamiltonian models and semi-empirically refined *ab initio* results. Technically, we need to maximize the success rate of energy level matches between the Ames-2 PES based predictions and CDSD models.

Before 2020, we have tried several approaches at Ames but all had failed to give satisfactory energy level matches for $^{12}C^{16}O_2$ beyond 20,000 cm^{-1}. The last trial took three months to match the $^{12}C^{16}O_2$ J = 0 – 74 levels up to 19,000 – 19,500 cm^{-1}, still far from adequate for high temperature. For each vibrational state, first 5 levels of the *e* or *f* component were manually identified. In each cycle, the changes of local *B-D-H* constants at E_{J-4}, E_{J-2}, and E_J were utilized to predict E_{J+2}. The procedure was tedious and slow, involving hundreds of manual checks on the vibrational state coupling and crossings. After this practice, we concluded it is unfeasible to do the physically meaningful band-to-band matches for Ames-2 vs CDSD in the wavenumber range above 22000-24000 cm^{-1}. Machine learning might offer limited help at higher J's and energies below 22000 cm^{-1}, but that still seems unlikely for the whole picture at 3000 K. The main reason is that the vibrational state couplings are intrinsically different between Ames-2 and CDSD, and the differences grow very fast at higher energies. For example, many couplings computed from the semi-empirically refined Ames-2 PES do not exist in the CDSD effective Hamiltonian models, due to the lack of experimental data. The accuracy of Ames-2 PES at high energies would gradually degrades to original CCSD(T)/cc-pVQZ level [37]. With higher density of states, this will also lead to larger discrepancies between the two sets of energy levels, which make them more difficult to match. Please note that some polyad band labels in CDSD are also impacted by the intricate inter and intra polyad couplings, so not fully consistent. In short, level by level (manual or AI) matches are a dead end for 3000 – 4000 K applications. A new direction is needed.

In this work, we choose to reduce the *overall* difference between the CDSD and Ames predictions at high energies, by adjusting the Ames PES with respect to selected CDSD energy levels. The new Ames PES based energy levels are expected to have a higher success rate in the simplest 1-to-1 matches or replacement with CDSD levels. Spectroscopically, it is equivalent to reduce the related IR peak shifts from Ames line lists to CDSD line lists, but this systematic improvement has no guarantee for any specific bands or regions. The newly refined PES is denoted X01d, which has been used in the AI-3000K line list calculations reported in this work. See more details in next section.

On the other hand, the X01d PES refinement focused more on the higher energy region, which has partially sacrificed the accuracy at lower energy region. For example, the J=0 band origins in the range of 0 – 13000 cm^{-1} now have σ_{rms} = 0.12 cm^{-1}, vs. σ_{rms} = 0.01 cm^{-1} on Ames-2 PES. Such one order of magnitude larger deviations may also hurt the accuracy of computed intensities. To maintain the accuracy in the lower wavenumber region, the Einstein A_{21} coefficients of Ames-2021 296K line lists [60] are adopted to replace their counterparts in X01d PES based line lists. The Ames-2021 line lists were computed using the Ames-2 PES [43] and the best available DMS for CO_2, Ames-2021 [60].

Next we introduce the CDSD2019 levels used in the X01d PES refinement, then the refinement, and the procedure of the AI-3000K construction. The full intensity calculations involve two PES and two DMS. The data size reduction and efficient storage are improved upon the Ames-1000K style in 2014.

III.2 CDSD 2019 Rovibrational Energy Levels

The CDSD 2019 [45] is an updated version of the CDSD-296 [39] databank. The databank contains the calculated line parameters (positions, intensities, air- and self-broadened half-widths and their coefficients of temperature dependence, as well as air- and self- pressure-induced shifts) of the twelve

stable isotopic species of CO_2. The reference temperature is 296 K, and the intensity cutoff is 10^{-30} cm^{-1} /(molecule cm^{-2}). The data bank includes more than half a million lines covering the spectral range 345–14076 cm^{-1}.

Parameters of the effective Hamiltonian model [67] were fitted to the observed line positions taken from the literature. The sources of experimental line positions for all isotopic species are listed in Tashkun et al. [39,45]. The fitted parameters were used to calculate the CDSD2019 transition wavenumbers. They were also used to replace the energy levels computed using the X01d PES refinement (the base of AI-3000K list) under the following constraints: $J_{max} \leq 150$ and $E'_{max} = 24{,}000$ cm^{-1}. The highest polyad $P = 2\nu_1+\nu_2+3\nu_3$ involved in the calculations was 40. Each energy level was labeled with quantum numbers ν_1, ν_2, l_2, ν_3, r, J", c, as those adopted in HITRAN.

III.3. X01d PES refinement

More details of CO_2 PES refinements were reported in Refs. [37,43] In this work, 22 coefficients of 0-4th order short-range expansion terms in Ames-2 PES potential formula were refined with respect to selected CDSD levels. Starting from J=0 band origins up to 18000 cm^{-1}, higher J and higher energy levels were added step by step. The experimental data based CDSD levels are highly accurate and intrinsically consistent, but not all the extrapolated levels in CDSD share same consistency. It is unrealistic to expect a CDSD based refinement carrying a σ_{RMS} similar to that of Ames-2 refinement. The final refinement of X01d PES had σ_{RMS} = 0.53 cm^{-1} (weighted), or 0.71 cm^{-1} (unweighted) for 821 CDSD levels selected at J=0,1,2,10, 25, 40, 55, 70, 85, 100, 115, 130, and 145, up to 24,000 cm^{-1}. In the simplest 1-to-1 match, a majority of the energy levels computed on the X01d PES refinement agree with the CDSD energies to within ±2 cm^{-1}. This can be taken as the upper limit of the compatibility or consistency between current Ames and CDSD extrapolations at high energies, i.e., 1-2 cm^{-1}, based on CDSD oriented refinements.

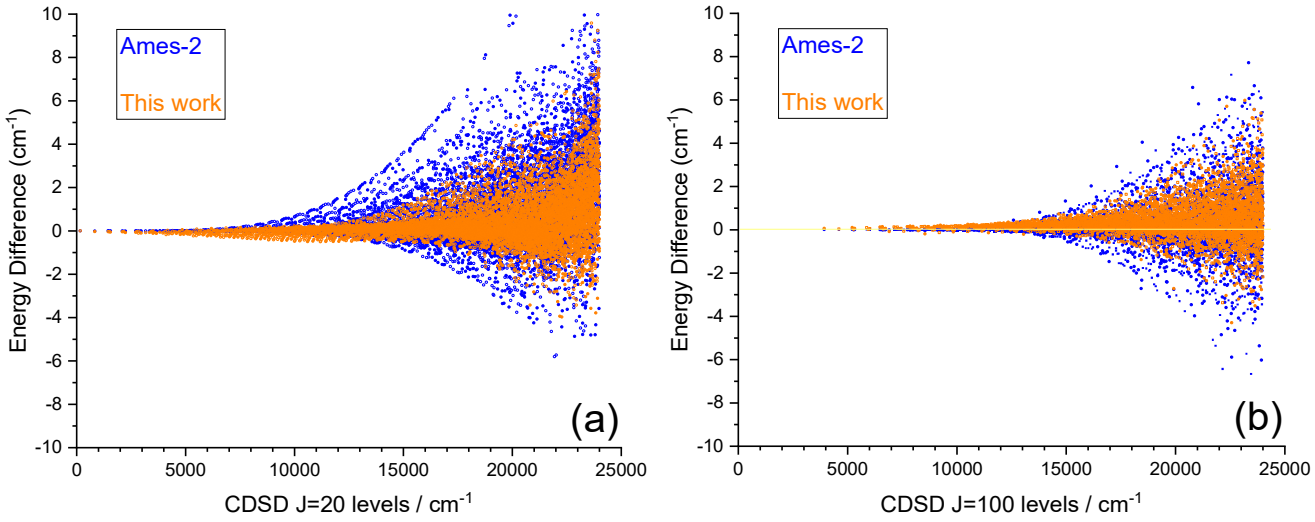

Figure 1. Compared to Ames-2 PES, the $\delta = E_{Ames} - E_{CDSD}$ energy differences are reduced. (a) J=20; (b) J=100.

Fig.1 shows a snapshot (*not* X01d) during the stepwise refinements. In panel *a*), the maximum $E_{Ames-2} - E_{CDSD}$ energy differences were reduced by more than 50% for J=20 levels at 18,000 cm^{-1}. In panel *b*), the differences at J=100 are also reduced, but not as significant as that at J=20.

Fig.2 reports the energy differences computed on the final X01d PES at J=0,1,2 and J=20,100. Compared to the intermediate snapshot in Fig.1b, more δE differences at J=100 (blue dots) are restricted to the range of ±2 cm^{-1}. The differences of J=20 levels are much smaller than those in Fig.1a on Ames-2 PES. But they rise more quickly in the range of 21,000 – 24,000 cm^{-1}, indicating there still exist systematic differences between X01d PES and CDSD models. We tried, but failed to further reduce them. Therefore, the CDSD reference energy level set for the refinement was limited to 24,000 cm^{-1}, not extended beyond 24,000 cm^{-1}. It is not clear if including higher order terms in refinement may help.

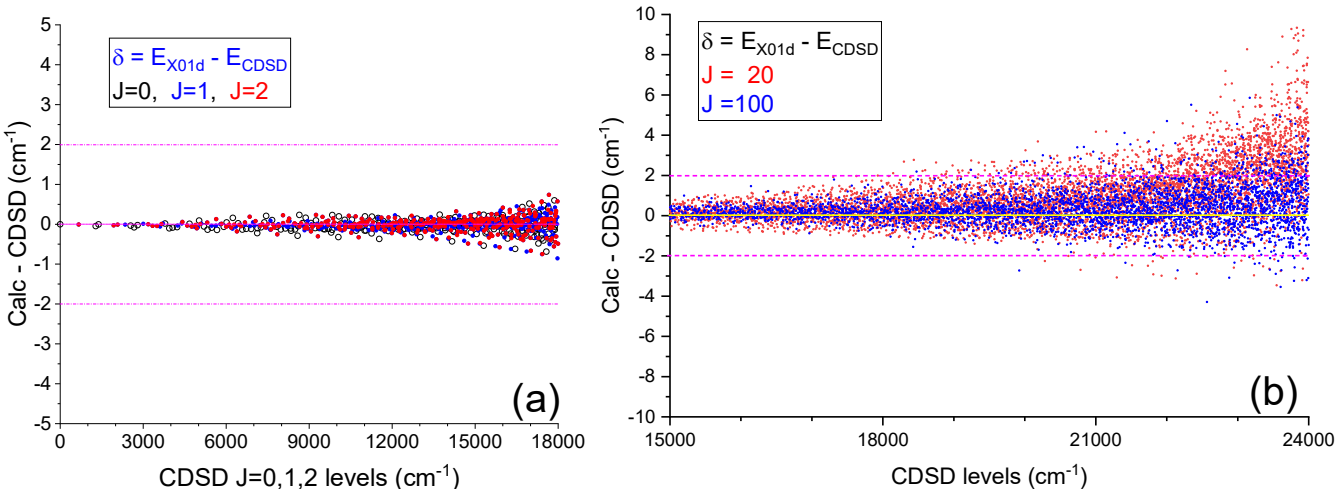

Figure 2. δE = $E_{X01d} - E_{CDSD}$ energy differences at selected J's. (a) J=0,1, and 2; (b) J=20 and 100.

The list of reference energy levels, input and output files of the X01d refinement, the X01d PES subroutine and coefficient files are reported as supporting information.

III.4. New DMS fit up to 40,000 cm^{-1}

In 2022, Ames-2021 DMS was reported as a major improvement for high accuracy CO_2 IR intensity calculation at 296K [60]. It was selected from Ames DMS fit series computed at the CCSD(T) level with aug-cc-pV(T,Q,5)Z bases and extrapolated to one-particle complete basis set limit. A 2nd diffuse function was added on O atoms to better describe the polarization orbitals due to external field, denoted 'davtq5zO'. The fitting σ_{rms} was 8.5×10^{-7} a.u. in the range of 0 – 30000 cm^{-1}, or 3.8×10^{-7} a.u. in the range of 0 – 15000 cm^{-1}. Using the Ames-2021 DMS and Ames-2 PES, the Ames-2021 296K IR line intensity computation has reached 1-4 permille level for both accuracy and uncertainty, when compared to NIST [68,69] and DLR [70] experiments on the 2001i and 3001i bands. Details of the Ames-2021 DMS can be found in Ref. [60]. But IR intensity calculation at 3000 K and above will involve calculations up to 36,000 cm^{-1}, or even higher.

Following the style of Ames-2021 DMS, extrapolated CCSD(T)/aug-cc-pV(T,Q,5)Z (denoted 'avtq5z') dipoles of 11155 geometries up to 40,000 cm^{-1} are fit to pseudo point charges on the O atoms with a 16th-order polynomial. Fitting σ_{rms} error is 5.1×10^{-6} a.u. for 22035 non-zero dipole components. Maximum deviation is 8.7 ×10^{-5} a.u., and averaged absolute deviation is 2.5×10^{-6} a.u. This is the dipole surface adopted in the major calculations of AI-3000K line list, denoted Ames-2021-40K. Fig.3a reports the number of dipole components and fitting σ_{rms} along rising energies. The number of non-zero dipole components is stable in the whole range of 0 – 40000 cm^{-1}, i.e., 450~650 in every 1000 cm^{-1}. Below

30,000 cm^{-1}, the fitting σ_{rms} error of Ames-2021-40K is 2-4 times as large as those of the Ames-2021 DMS, which was selected for 296 K IR intensity accuracy toward 0.1% level. Larger fitting σ_{rms} could lead to relatively larger uncertainty in intensity computations using the DMS. Therefore, it is a reasonable choice to upgrade the computed Einstein A_{21} of moderate to strong transitions to more reliable values reported in the Ames-2021 296K IR line lists, which were computed using the Ames-2 PES and Ames-2021 DMS, i.e., the best PES and DMS available for CO_2 rovibrational IR studies.

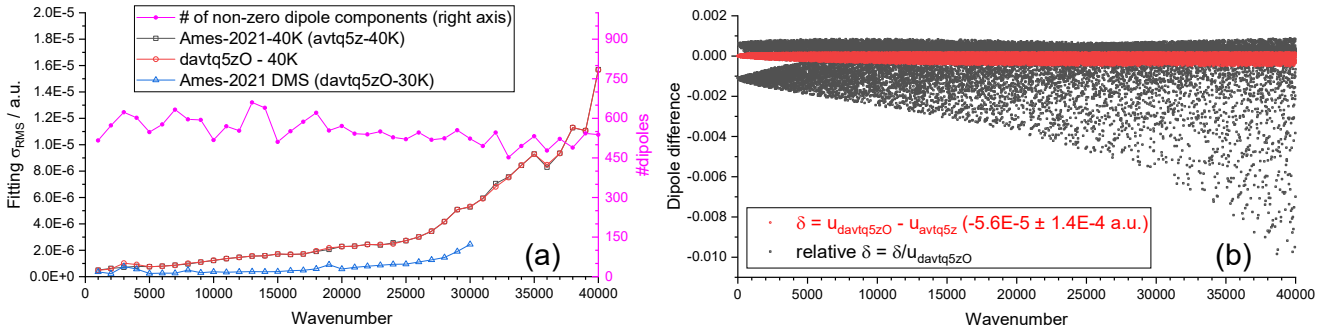

Figure 3. (a) number of dipole components and fitting rms (in a.u.) at every 1000 cm^{-1}; (b) difference between davtq5zO and avtq5z dipole fits are shown by red dots, relative differences with respect to davtq5zO dipoles are black open squares. Note the absolute and relative differences share the *y* axis, but have different units.

The choice of 'avtq5z' dipole fit for Ames-2021-40K DMS, instead of the 'davtq5zO' dipole fit, is based on following observations, and intended for tests. In Fig.3 and Fig.6 of Huang et al [60], the "avtq5z40KF" (aka. 'avtq5z' in this work) based intensities are only 0.7-1.2‰ less than the "davtq5zO30KF" (aka. 'davtq5zO' in Ames-2021 DMS) based intensities for CO_2 2001*i* and 3001*i* bands. They are essentially fully equivalent. We believe the 'davtq5zO' dipole fits are probably more reliable, while their differences at low energies are rather small, at least for strong bands. The dipole component difference $\delta = \mu_{davtq5zO} - \mu_{avtq5z}$ are plotted in Fig.3b as red dots, with mean ± σ_{rms} = -5.6×10^{-5} ± 1.4×10^{-4} a.u.. The relative differences, $\delta/\mu_{davtq5zO}$, are plotted as black open circles, with mean ± σ_{rms} = -0.3‰ ± 1.1‰. This suggests the associated intensity differences should be also around 1‰, averaged for most bands up to 40000 cm^{-1}. Please note the absolute and relative differences share the *y* axis, but have different units. Currently, experiment and theory are still working towards 1 permille (or 1‰) accuracy and uncertainty at 296 K for strong bands below 10,000 cm^{-1}. According to our knowledge, no experimental intensity data previously reported at high temperature carry accuracy and uncertainty good enough to provide an accuracy check at permille level. Therefore, the 'avtq5z' and 'davtq5zO' based dipole fits can be treated equivalent for our intensity calculations in the range of 15,000 – 40,000 cm^{-1}.

As pointed out in Huang et al. [60], the best theoretical intensity calculation needs both the best PES and the best DMS. Future CO_2 DMS should focus on reducing the fitting errors beyond 30,000 cm^{-1}. One potential improvement on AI-3000K line list is to recompute the transition intensities up to 30,000 cm^{-1} using the X01d PES and the Ames-2021 DMS. But the intensity accuracy loss caused by less accurate DMS fits is still difficult to estimate, partially due to the lack of high quality experiment intensity data. On the other hand, we do not plan to repeat the calculation using the Ames-2 PES and the Ames-2021-40K DMS, because it defies the original purpose of X01d PES refinement.

III.5 Procedure of AI-3000K construction.

The AI-3000K line list includes the four most abundant isotopologues: 626, 636, 628, and 627. Their individual line lists were computed up to 36000 cm^{-1} or 40000 cm^{-1}, and each will easily occupy dozens of terabytes on disc. To generate a line list suitable for IR simulations in a wide range of temperatures, the contribution and importance of every transition needs to be estimated at five temperatures: 296K, 1000K, 2000K, 3000K, and 4000K, so that the weakest and negligible lines can be excluded. After the J=0-250 (626) or J=0-200 (636, 628, and 627) rovibrational calculations for wavefunction and transition dipole moment using the X01d PES + Ames-2021-40K DMS, our step 1 is to compute the sum of intensities S_{total} in every 0.01 cm^{-1} interval using all transitions with intensities stronger than 10^{-50} cm^{-1}/molecule.cm^{-2} at 296K, or 10^{-40} cm^{-1}/molecule.cm^{-2} at the other 4 temperatures, assuming 100% abundance for each isotopologue. In step 2, five intensity cutoffs are determined separately for each 0.01 cm^{-1} interval to ensure the intensity sum of transitions stronger than the cutoffs has reached 99.99% of S_{total} at 296 K and 1000 K, or 99.95% at 2000 K, or 99.9% at 3000 K and 4000 K. For each transition, five unit integers are used to indicate its importance at five temperatures, e.g., "00111" means this transition can be ignored at 296K and 1000K (the two '0'), but should be included in 2000 K, 3000 K, and 4000 K lists (three '1'). A line is selected for AI-3000K if *any* of the five integers equal to 1. Note all lines with 296 K intensity stronger than 10^{-42} cm^{-1}/molecule.cm^{-2} are also selected. All the selected lines are written out in step 2.

A critical procedure of quality control runs along with step 2, before the generation of the final line lists for individual isotopologues. That is to identify and remove the numerical intensity noises and bad wavefunctions generated during the rovibrational variational calculations up to 40000 cm^{-1} (for 626) or 36000 cm^{-1} (for 636, 628 and 627). The simulated IR spectra from simple Gaussian convolution with σ = 1 cm^{-1} and 0.1 cm^{-1} are scanned carefully to identify suspicious peaks or fake intensity lines in the computed line lists. The rovibrational energy levels associated with those unreliable transitions are also marked as "unreliable", which are usually at high energies. Re-run step 1 by excluding *any* lines involving those "unreliable" levels, and re-run step 2 again to generate a new line list. This accomplishes one cycle of "purification". Then the cycle is repeated on the new, filtered line list, because there may be additional bad lines appearing after stronger noises have been removed. It usually took 2 – 4 cycles to reach a satisfactory result. However, it should be noted that this purification procedure had only very small intensity reduction around 20,000 cm^{-1} at 3000 K. No other differences were found at lower temperature or lower wavenumber range, i.e., essentially zero impact for convoluted IR spectra below 18,000 cm^{-1}. Most bad lines were found above 24000 cm^{-1}, e.g., 30,000 – 36,000 cm^{-1}. This supports the stability of AI-3000K intensity calculations and indicates the wavefunction defects are mostly localized.

After all the "unreliable" levels and transitions have been excluded, step 3 re-runs the line list generation in the range of 0 – 20,000 cm^{-1}, with the finalized intensity cutoffs taken as "exact" for the 0.01 cm^{-1} intervals. For example, if a cutoff for 3000 K was 10^{-36} cm^{-1}/molecule.cm^{-2}, those transitions carrying intensities between 10^{-40} and 10^{-36} cm^{-1}/molecule.cm^{-2} will be excluded from that 0.01 cm^{-1} interval. Effectively, this will slightly reduce the S_{total}, but the reductions are < 0.01% at 1000 K, < 0.05% at 2000 K, and < 0.1% at 3000 K and 4000 K. It will not impact the quality of line lists. Now the generated IR line list is ready to mix with the IR line lists of other minor isotopologues.

To investigate the convergence and reliability of AI-3000 K, two IR line lists have been computed for the main isotopologue, $^{12}C^{16}O_2$, one with E' up to 36000 cm^{-1}, and the other with E' up to 40,000 cm^{-1}. The E' cutoffs lead to different S_{total}, so it also has an influence on the intensity cutoffs. Lower value of

the two intensity cutoffs was adopted to ensure 99.9-99.99% intensity conservation for both line lists. In most (but not all) cases, the intensity cutoff for the 40,000 cm^{-1} list is lower than that of the 36,000 cm^{-1} list. See next sections for detailed comparisons between the two lists.

Step 4 is to combine the 4 isotopologue line lists into a half "natural" CO_2 list with terrestrial abundances. In each 0.01 cm^{-1} interval, the thresholds adopted for the conservation of new S_{total} are 99.99% at 296 K and 1000 K, 99.95% at 2000 K, 99.9% at 3000 K, and 99% at 4000K. Compared to the thresholds in step 2 and step 3, the reduction at 4000 K from 99.9% to 99% is based on our analysis showing that convergence is probably insufficient at 4000 K. We estimate the uncertainty at 4000 K is at least 3-5%, i.e., much larger than 1%. Including more weaker lines cannot help bring back the missing intensities.

III.6 Data storage, number of lines, and partition function

The combo line list generated from step 4 covers the spectra range from 0 to 20,000 cm^{-1}. In step 5, it is saved into 2000 plain text files, each covering 10 cm^{-1}. Each transition is stored as 24 decimal digits (0-9): 1 digit for isotopologue index (1-4) and parity of upper and lower levels, 3 digits for upper state J', 2 digits for ΔJ and importance indicators at five temperatures, 8 digits for Einstein A_{21} coefficients with 6 significant figures, and 2 × 5 digits for the eigenroot sequence numbers of upper and lower levels in their *JPS* symmetry blocks. In this step, the A_{21} values in Ames-2021 296 K IR line lists [60] are adopted to replace their counterparts in those transitions with $E' < 15{,}000$ cm^{-1}, and S_{296K} (100% abundance) > 10^{-36} cm^{-1}/molecule.cm^{-2} (626), or 10^{-34} cm^{-1}/molecule.cm^{-2} (636, 628, and 627). The plain text files are compressed into .tgz format for more efficient storage.

Table 1 summarize the number of transitions in the AI-3000K line list from 0 to 20,000 cm^{-1}. In total there are 36 billions of IR transitions, occupying ~400 GB disc space. 75% of the lines belong to the main isotopologue 626. On average, a transition takes 11 bytes in .tgz file storage. The numbers of lines at 4000 K are only a fraction to half of those at 3000 K. As mentioned, using higher threshold (e.g. 99.5%) did not bring them in line with the 3000 K numbers.

Table 1. IR transitions in the AI-3000K line list, including 4 isotopologues.

#lines to include	$^{12}C^{16}O_2$ (626)	$^{13}C^{16}O_2$ (636)	$^{16}O^{12}C^{18}O$ (628)	$^{16}O^{12}C^{17}O$ (627)
296 K	8,679,292	4,102,781	9,187,117	5,896,321
1000 K	574,267,343	129,459,222	208,009,376	94,383,807
2000 K	11,581,289,410	1,259,622,929	2,252,742,848	717,929,106
3000 K	27,397,362,378	2,691,372,006	4,578,190,786	1,294,391,142
4000 K	16,955,873,906	815,640,117	1,041,707,073	203,707,345
Sum	27,548,493,437	2,780,854,018	4,801,316,888	1,418,062,103
Total	36,548,726,446			

To convert the compressed line list files back into full line list, the J=0-250 (or 200) rovibrational energy level lists are required, plus a separate file containing the zero-point energy and partition function values of 4 isotopologues. The rovibrational energy level lists include both X01d PES based energies up to 36,000 cm^{-1} or 40,000 cm^{-1}, and CDSD2019 levels up to 24,000 cm^{-1}. They are listed side by side, so that users can choose either set of values to use, or even customize the choices for specific spectra range. According to our tests, CDSD based line positions have significantly improved the agreement with high resolution IR experiments at high temperatures. See next section for example.

Partition function values of $^{12}C^{16}O_2$ are compared in Table 2, and sorted by decreasing order at 4000 K. First we note the differences between X01d (40K) and CDSD-4000 [50] at 3000 K and 4000 K are as small as 0.0043% and 0.067%, respectively. Across the table, the agreement at 296 K is better than 99.998%. The differences at 1000K are also less than 0.004%. From 1000 K to 2000 K, the relative differences between Effective Hamiltonian model based extrapolations (HITRAN and TIPS) and semi-empirical calculations (X01d and UCL-4000, which is Ames-1 PES based) rise up to 0.18%, i.e., an increase of 4 times. It further rises to 1.25% at 3000 K, then 2-5% at 4000 K. Between UCL-4000 and this work, the difference is less than 0.3% at 3000 K, near 3% at 4000 K, and 8.6% at 5000 K. The impact of 36000 cm^{-1} vs 40000 cm^{-1} cutoff is only 0.17% on X01d PES, so the E' cutoff might not be the major reason behind that 3% discrepancy. As we have checked, the $J = 230$ (not shown) vs $J = 250$ difference is only ~0.04%. Currently, the difference between UCL-4000 and this work is tentatively attributed to the Ames-1 vs X01d PES differences, but it is unclear which high energy levels or regions are primarily affected. Although it will not impact the comparison and analysis presented in this paper up to 3000 K, a separate study will be needed to ensure the convergence at higher temperatures. Note the differences between X01d(40K) and Ames-2 PES are 0.001, 0.01, 0.01, 0.14 and 6.0 at the five temperatures, respectively, i.e., the relative differences are all less than 0.002%.

Table 2. Partition function values of $^{12}C^{16}O_2$, compared to earlier studies.

$Q(^{12}C^{16}O_2)$	296K	1000K	2000K	3000K	4000K
CDSD-4000 (44K) [50]				114762	378338
Ames-2 PES (40K)	286.0979	2838.5824	24622.4657	114757.1426	378089.4113
X01d (this work, 40K)	286.0968	2838.5914	24622.4771	114757.0085	378083.4302
X01d (this work, 36K)	286.0968	2838.5914	24622.4763	114750.0436	377446.8213
UCL-4000 (36K) [53]	286.0983	2838.5737	24622.0857	114428.1111	367222.6396
HITRAN [66] (hitran.org)	286.0938	2838.4728	24578.6085	113009.0950	359312.8600
TIPS 2017 [71]	286.09	2838.5	24579	113010	359310

IV. AI-3000K : Convergence Tests

Unless specified, default 'AI-3000K' in following discussions refers to the line list including 4 isotopologues with E'/E'' (626) up to 40,000 cm^{-1}, all rovibrational levels in the range of 0 – 24,000 cm^{-1} are updated by CDSD2019 energies, and the A_{21} coefficients for transitions with E'<15,000 cm^{-1} and $S_{296K} > 10^{-36}$~10^{-34} cm^{-1}/molecule.cm^{-2} are replaced using Ames-2021 296 K line list values. Therefore, for most transitions at 296 K, the line position accuracy can refer to that of CDSD 2019 [45], and line intensity accuracy can refer to that of Ames-2021 296K IR line list reported in Huang et al. (2022) [60]. More statistical plots are reported in supplementary file 'README'.

IV.1 Overview and Isotopologue Contribution

In Fig.4, left panels *a*) and *b*) show the overview spectra of 4 isotopologues separated at 1000 K (top *a*) and 3000 K (bottom *b*). Above 5000 cm^{-1}, the main isotopologue (626) intensity is the strongest at both temperatures. At 3000 K, it is interesting to observe that in the range of 12,000 cm^{-1} to 20,000 cm^{-1}, the asymmetric 628 isotopologue absorption is stronger than that of the symmetric 636 isotopologue, which is the 2nd most abundant of all CO_2 isotopologues,. Near 20,000 cm^{-1}, the S_{627} intensity is also stronger than S_{636} intensity. The 0 – 5000 cm^{-1} region is enlarged in right panels *c*) and *d*). At 1000 K, 628

and 627 absorptions dominate the range of 1200 – 1500 cm^{-1} and 2600 – 2700 cm^{-1}. But at 3000 K, the 626 intensity is the strongest everywhere. Note the data points in Fig.4 use the intensity sum of 10 cm^{-1} intervals, which is sufficient for the qualitative analysis in this section.

Obviously, 636, 628, and 627 isotopologues must be included for IR analysis and simulations at low energy or at temperatures below 1500 K – 2000 K. At 3000 K and above, their contributions are trivial and can be safely ignored in most spectral regions, unless one really needs highly accurate intensity converged better than 99% – 99.9%. For example, in the scale of Fig.4d the contribution from isotopologues #2 - #4 at 3000 K is only visible around 1350 cm^{-1}. It is barely detectable at 4000 K.

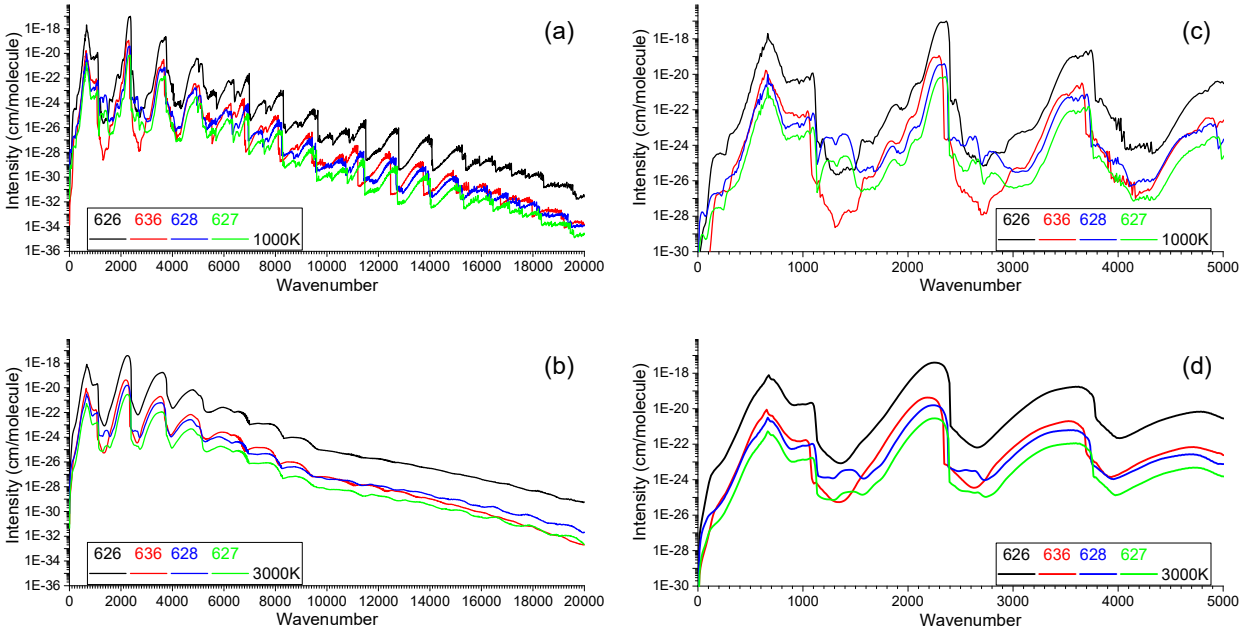

Figure 4. IR simulations for 4 CO_2 isotopologues in AI-3000K line list: (a) overview at 1000 K; (b) overview at 3000 K; (c) 0-5000 cm^{-1} at 1000 K; (d) 0-5000 cm^{-1} at 3000 K. Intensity data are summed over each 10 cm^{-1}.

Compared to UCL-4000, the 626 black lines in Fig.4b have a slope generally consistent in the range of 11,000 – 20,000 cm^{-1}, not as flat as shown in the Fig.4 of Yurchenko et al (2020) [53]. Those extra IR intensities in UCL-4000 at the high end of wavenumbers are probably related to the irregular intensity peaks of cold band series, $n110i$, where n = 7 – 14 and i = 1,2,…,n+1. Those peaks can be easily identified at 300 K [60] and 500 K [53]. See Fig.13 of Huang et al. (2022) [60] for more details and discussions about the potential source of intensity noise in UCL-4000.

Another difference between AI-3000K and UCL-4000 is more significant in the trough regions below 10,000 cm^{-1}. See Fig.5. From 2000 K to 3000 K, or from 3000 K to 4000 K, the intensity increments of AI-3000K list are much greater than those of UCL-4000, especially in the range of 1300 – 1350 cm^{-1}, and 2600 – 2700 cm^{-1}. From 3000 K to 4000 K, the intensity increments of UCL-4000 in those troughs are very small or hard to find, as shown in the Figure 4 of Yurchenko et al. (2020) [53]. This is mainly caused by the E''<16,000 cm^{-1} cutoffs adopted in UCL-4000 line list. See Sec.IV-3.

IV.2 Impact of E' cutoff

The overview spectra in Fig.5 compare two $^{12}C^{16}O_2$ line lists from 296 K to 4000 K, to investigate the impact of E' cutoffs. The list with E'<36,000 cm^{-1} cutoff ('36K') is plotted as solid lines while the list with E'<40,000 cm^{-1} cutoff ('40K') is plotted as dotted lines. At 1000 K, dotted and solid red lines completely overlap with each other in the whole range up to 20,000 cm^{-1}. At 2000 K, starting from 15,000 cm^{-1}, the blue dotted line is separated from the blue solid line. At 3000 K, green dotted and solid lines start to differ near 9000 cm^{-1}. At 4000 K, purple dotted line is stronger than solid line in most regions, except the peak regions below 5000 cm^{-1}. Therefore, it is concluded that the 36,000 cm^{-1} cutoff is insufficient for 4000 K analysis, while the 40,000 cm^{-1} cutoff seems good for 3000 K IR simulations up to 9000 cm^{-1}.

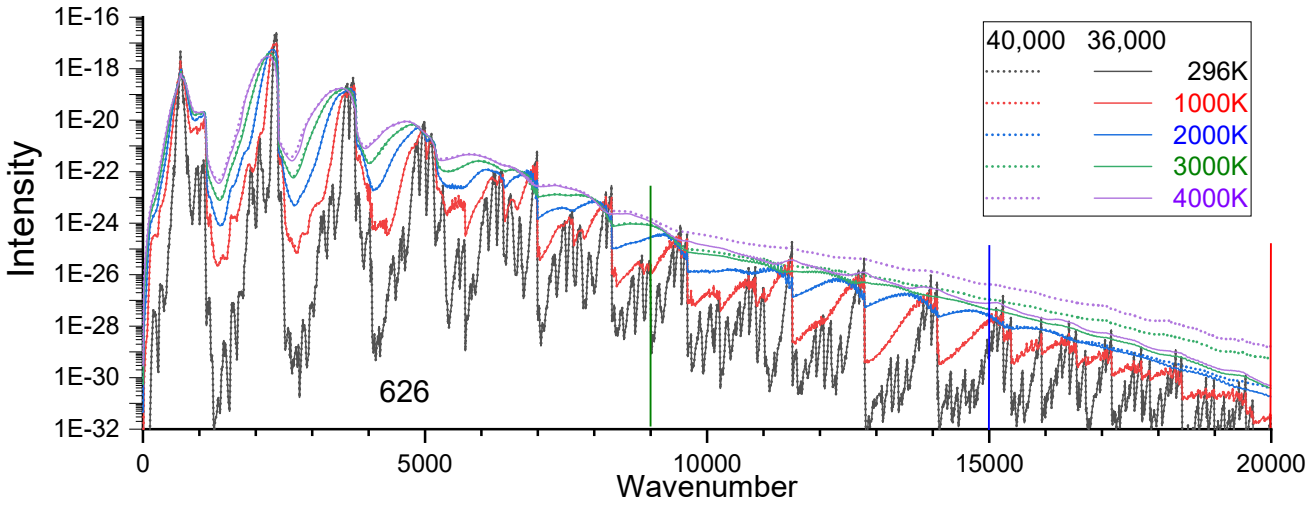

Figure 5. Overview spectra of $^{12}C^{16}O_2$ in AI-3000K from 1000 K to 4000 K, with E'/E"< 36000 cm^{-1} or E'/E"<40000 cm^{-1}. Intensity data are summed over each 10 cm^{-1} range.

The convergence defect of E'<36,000 cm^{-1} is also evident in the range of 10,000 to 20,000 cm^{-1}. From 2000 K to 4000 K, the separations between solid lines are much smaller than those between dotted lines. However, it is difficult to estimate the intensity accuracy of AI-3000K in the range higher than 15,000 cm^{-1} ($T \geq 3000$ K) or higher than 10,000 cm^{-1} ($T \geq 4000$ K). For these ranges, a 20% intensity uncertainty could be considered an acceptable prediction at 4000 K, especially in some sensitive regions.

Fig.6 gives three examples for the impact of E' cutoff, with linear scale of intensity. In panel *a*, difference between S_{40K} and S_{36K} is small at 3000 K (green lines), e.g., 2-3% at 50 cm^{-1}. At 4000 K, S_{40K} is 20% stronger than S_{36K}. In panel *b*, the S_{40K} vs S_{36K} difference at 3000 K goes from 2% at 2500 cm^{-1}, 8% at 2600 cm^{-1}, to 17% at 2700 cm^{-1} and 35% at 2800 cm^{-1}. At 4000 K, the corresponding differences are 22%, 39%, 60% and 101%, respectively. This is one of the most sensitive spectra ranges of CO_2 that we will keep monitoring at high temperatures. The comparison in panel *c* is at 10,000 cm^{-1}. The S_{40K} vs. S_{36K} difference is less than 1% at 2000 K, 30-35% at 3000 K, and as large as 140% at 4000 K.

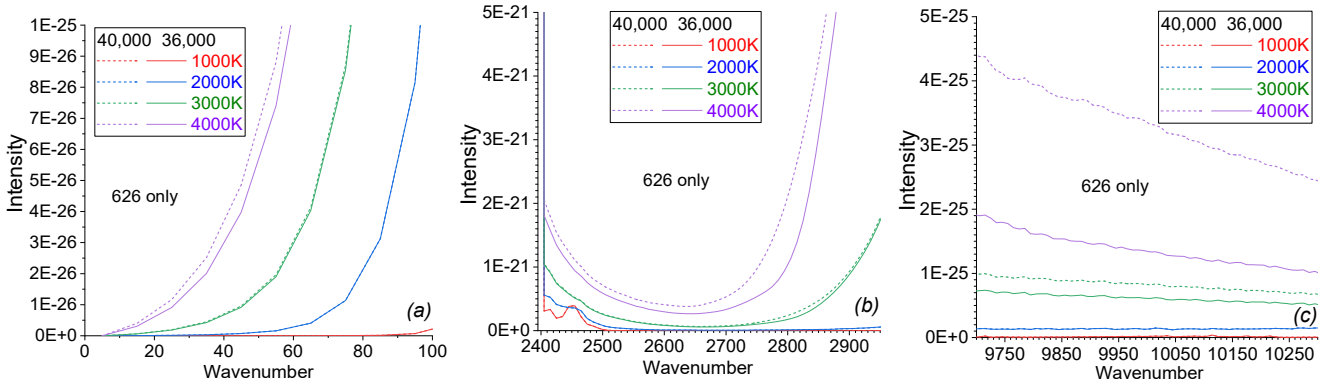

Figure 6. Impact of E' cutoff (a) below 100 cm^{-1}; (b) 2500 – 2900 cm^{-1}; (c) 10000 cm^{-1}. Intensity data are summed over each 10 cm^{-1} range. Solid lines represent E'<36K cm^{-1} list, while dotted lines represent E' < 40K cm^{-1} list.

It should be noted that both Fig.5 and Fig.6 use intensity sum over 10 cm^{-1} intervals. However, 1 cm^{-1} or 0.1 cm^{-1} based comparisons not necessarily lead to larger relative differences. Fig.7 reports the ratio of intensity in S_{40K} associated with E' = 36000 – 40000 cm^{-1}, or $\Delta S = S_{40K} - S_{36K}$, with intensity data summed over every 1 cm^{-1}. With log10 scale in Fig.7a and regular linear scale in Fig.7b, we can quantitatively estimate the intensity convergence with respect to E' cutoff at specific wavenumber. At 1000 K (blue dots), the ratio of ΔS is less than 10^{-6} in the range of 0 – 12,500 cm^{-1}, and less than 5×10^{-4} at 20,000 cm^{-1}. The convergence at 1000 K is fully satisfactory up to 20,000 cm^{-1}, with either E' cutoffs. At 2000 K, the ratio is less than 0.01, or 1%, in the range of 0 – 9650 cm^{-1}. Then it increases to 10% at 15,000 cm^{-1}, and 50+% at 20,000 cm^{-1}. These ratios allow us to estimate that the convergence at 2000 K should be better than 97-99% up to 15,000 cm^{-1} for S_{40K}, or better than 98-99% up to 10,000 cm^{-1} for S_{36K}. The blue vertical line in Fig.5 marks the estimated 'reliable' limit of S_{40K} at 2000K.

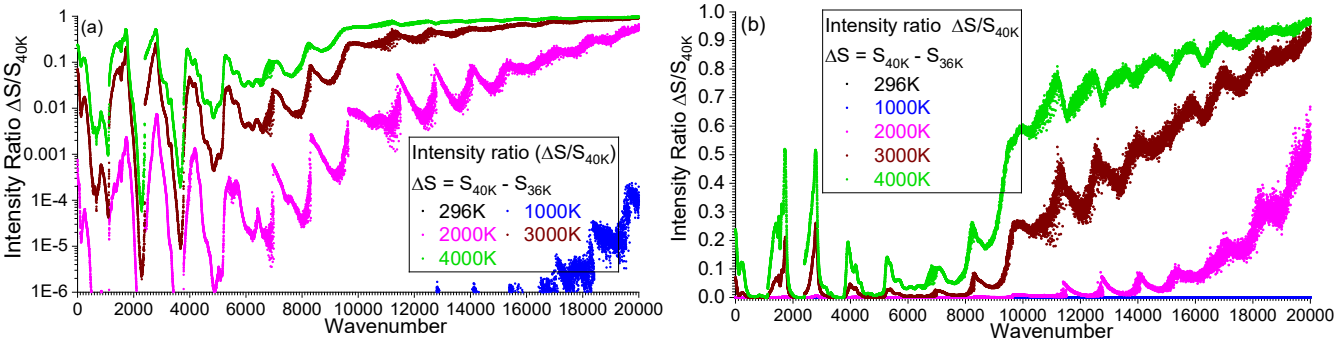

Figure 7. Ratio of intensity in S_{40K} from transitions with E' = 36000 – 40000 cm^{-1}. (a) log10 scale; (b) regular scale, 0.0 – 1.0. Intensity data are summed over each 1 cm^{-1} range.

At 3000 K and 4000 K, the ratio of ΔS rises quickly from 5-20% near 9000 cm^{-1} to 50-80% around 14000 cm^{-1}. The ΔS contribution further increases in the range of 15,000 – 20,000 cm^{-1}. Obviously, neither S_{36K} nor S_{40K} is sufficient for IR simulations above 10,000 cm^{-1}, if they need to be converged better than 90%. At 3000 K, S_{36K} may meet the 90% convergence criteria below 9000 cm^{-1}, except two sensitive ranges of 1400 – 1800 cm^{-1} and 2600 – 2900 cm^{-1} where the ratio of ΔS is as high as 0.2 – 0.3, or 20-30%. We estimate that S_{40K} may meet the 90% convergence criteria in the whole range of 0 – 9000 cm^{-1} at 3000 K, but only partially at 4000 K because the ΔS ratios in the two sensitive ranges rise to 0.5, or 50%.

IV.3 Impact of *E*'' cutoff

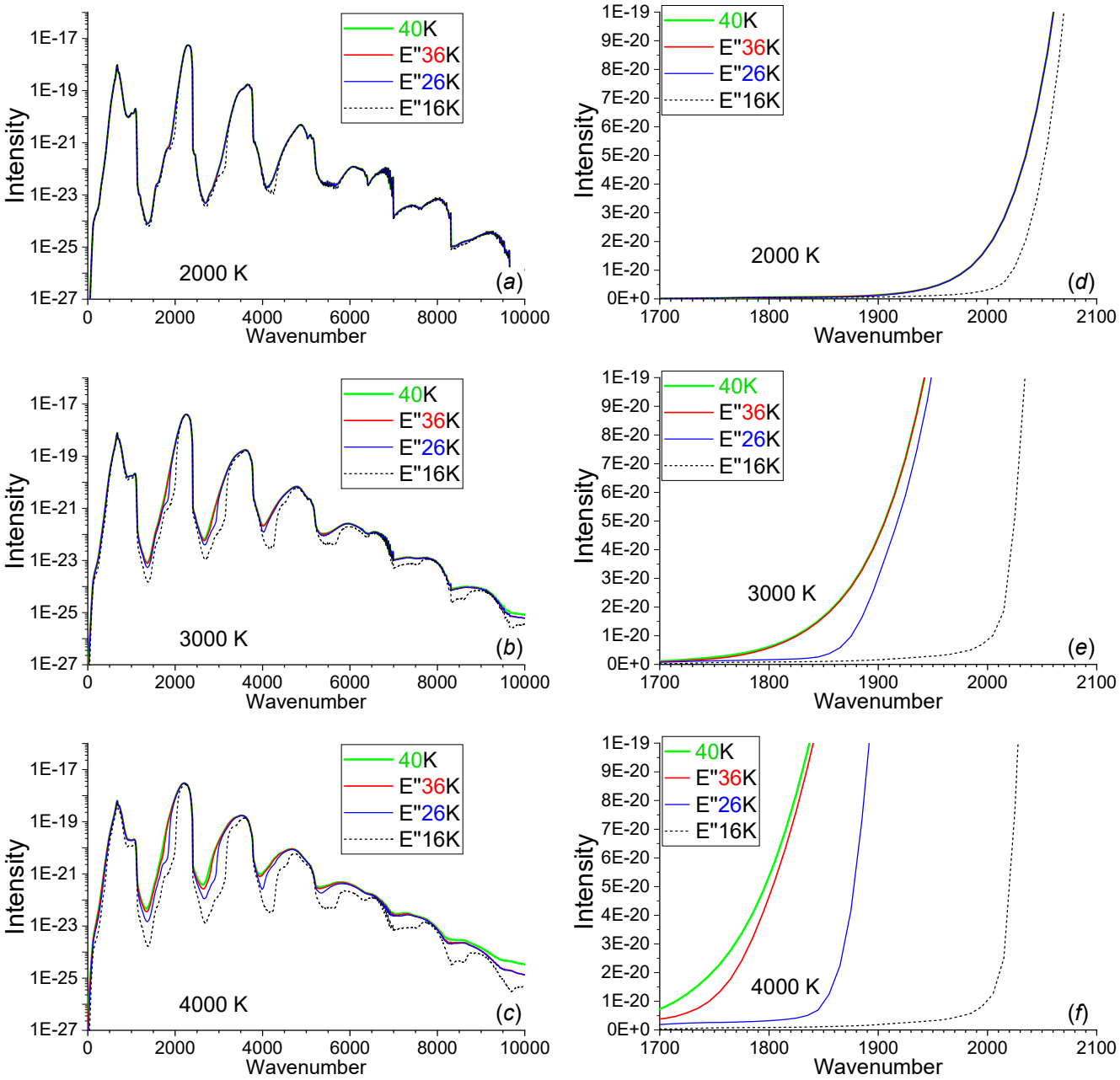

Figure 8. Impact of *E*'' cutoff in S_{36K} line list of $^{12}C^{16}O_2$. The full S_{40K} (green) is given along for reference. Panels *a* and *d*: 2000 K; panels *b* and *e*: 3000 K; panels *c* and *f*: 4000 K. Panels *a,b,c* are overview, and *d,e,f* are 1700 – 2100 cm^{-1}.

The top panels *a-c* of Fig.8 illustrate the impact of the *E*'' cutoff in overview from 0 to 10,000 cm^{-1}, using intensity sum of 10 cm^{-1} bins. To separate the *E*' and *E*'' cutoff impacts, the AI-3000K line list is filtered by *E*'=36,000 cm^{-1} and three *E*'' at 16,000 cm^{-1} (16K, black), 26,000 cm^{-1} (26K, blue), and 36,000 cm^{-1} (36K, red). The full S_{40K} intensity is plotted in green lines for comparison. At 2000 K, the separation between the black and blue lines are clear in troughs and shoulders, while the red and green lines are barely distinguishable. An extreme example is given in panel *d* at 2010 cm^{-1}, where *E*''(26K) leads to intensity 4-5 times stronger than that of *E*''(16K). This suggests the following in the illustrated range: 1)

the E"<16,000 cm^{-1} cutoff is not always adequate at 2000 K; 2) E"<26,000 cm^{-1} or E"<36,000 cm^{-1} are nearly equivalent at 2000 K; 3) difference between E'<36,000 cm^{-1} and E'<40,000 cm^{-1} is negligible at 2000 K.

At 3000 K, the separation between blue and black lines are significant in many regions of panel *b*. The intensity ratio of E"(26K)/E"(16K) at 2010 cm^{-1} rises to ~20:1, as partially shown in panel *e* of Fig.8. The separation between red and blue lines is also noticeable at several shoulders in panel *b*. The intensity ratio of E"(36K)/E"(26K) is about 6:1 at 1840 cm^{-1} (panel *e*). The separation between green and red lines is very small in most regions of panels *b* and *e*, while the full S_{40K} intensity can be 35% stronger than that of E"(36K) at 2800 cm^{-1} or near 10,000 cm^{-1}. It is consistent with the E' analysis in previous section.

Comparison at 4000 K is given in panels *c* and *f*. The separation between red and blue lines is significant in many regions, e.g., the intensity ratio of E"(36K)/E"(26K) reaches 10~20:1 between 1780 cm^{-1} and 1850 cm^{-1}. The separation between green and red lines is also clear, but not that large. The full S_{40K} intensity is two times as large as that of E"(36K) at 1715 cm^{-1} and 2790 cm^{-1}, while the S_{40K}/S_{36K} ratio is generally in the range of 1.0 – 1.1, for 70% of the wavenumber range from 0 to 8000 cm^{-1}.

In summary, the E" cutoff is the foremost factor impacting the spectra convergence under 10000 cm^{-1}, especially near the trough regions. E"<36,000 cm^{-1} may be acceptable at 3000 K for many spectra regions below 10,000 cm^{-1}, but probably not adequate for 4000 K, either. Further studies are required to confidently converge a semi-empirical IR line list above 3000 K, which will definitely require both E' and E" cutoffs going beyond 40,000 cm^{-1}.

V. Compared to Shock Tube Experiment Spectra

After convergence checks, AI-3000K line list needs to be further evaluated against reliable experimental IR spectra measured at high temperatures. Experiments with middle to low resolution can provide qualitative reference for overall estimation of intensity accuracy or deficiency. Examples include Bharadwaj and Modest (2007) [61] and Evseev, Fateev and Clausen (2012) [62], which we compared to Ames-1000K in Ref. [52]. But only high-resolution experimental spectra can provide quantitative, or at least semi quantitative guidance for line position and intensity improvements.

In 2017, Mulvihill and Petersen [72] reported high-resolution (0.001 cm^{-1}) shock tube IR spectra of CO_2 diluted in Ar (7.509%), measured in the range of 2188.8 – 2191.8 cm^{-1} with temperature from 1158 K to 2017 K, and pressure from 5.1 kPa to 108.4 kPa. They found closest agreement with HITEMP2010 [51]. Near 50 spectra were reported as ORIGIN graphs in their supplementary .doc file, with measured spectroscopic data built in. In this study, the data is extracted and compared to AI-3000K, HITEMP [51], and UCL-4000 [53] line lists. Due to various uncertainties in experiment, calculation, and line shape modeling, these comparisons are largely primitive. The main goal is to check the agreement level, report discrepancies, propose explanations, and suggest fixes.

The shock tube simulations [72] were generated using a Voigt profile. The extent of the line wings was determined using a formula that has been used in the past by the EXOMOL group : 200.×(γ_L + γ_D), where γ_L is the HWHM pressure broadening width and γ_D is the HWHM Doppler width. It is generally assumed that the far wings of molecular lines are non-Lorentzian due to the effects of line mixing and other limitations of the impact approximation in collisional broadening. These effects are not considered here and the formula that limits the extent of the line wings is designed to capture almost 100% of the line

opacity. The far wings of these lines are not significant in these simulations as the pressures measured in the experiments are modest and very extended line wings do not play a significant role in the overall opacity.

The partition function used for the main isotopologue of CO_2 was derived from UCL-4000. As shown in Table 2, a direct comparison with newer data from this work and the HITRAN2020 shows agreement in the region of these simulations - up to 2000 K. For the other three isotopologues, HITRAN values were also used for the partition functions. The theoretical line strengths in all cases [HITEMP 2010 : UCL-4000 : current work] are weighted by the relative terrestrial abundance of each isotope in order to be compatible with the shock tube experiments.

The shock tube experiments were conducted in a CO_2-Ar mixture with the Ar concentration at 92%. In order to conduct the simulations, it was necessary to provide CO_2-Ar pressure broadening widths. After searching the literature for available information, a table of half-widths was assembled that depended only on the value of J'' or |m|, which is branch dependent, while the value of the CO_2 self-broadening widths was taken from HITRAN data by using an average over values for J'', or in the case of HITEMP 2010 the self-broadening data was already available in the line list.

The sources for the Ar-CO_2 widths were taken from several papers (see below). In Mulvihill and Petersen [72] (Figure 10), they report the results of a number of investigations of CO_2-Ar broadening as a function of |m| where $m = J'' + 1$ for R branch lines, $m = -J''$ for P branch lines and $m = J''$ for Q branch lines. For higher values of J'', data was taken from a paper by Lee and colleagues [73] which also quotes other references. Another paper by Buldyreva and Chrysos [74] compares a semiclassical model of CO_2-Ar widths and shows that the available measurements agree well with their theoretical predictions at least for lower temperatures. The agreement between theory and experiment decreases at higher temperatures.

The value of 'n' - the exponent in the temperature dependence of the pressure width - had to be estimated from data taken mainly at temperatures lower than the shock tube experiments, although papers such as Lee et al. [73], Thibaullt et al. [75], and Wooldbridge et al. [76] are examples of studies that include a few measurements of isolated lines taken at higher temperatures. A final decision on the value of n to use and its variation with J'' was based on an estimate made from all the available data, particularly data from Lee, et al. [73] and Thibault et al. [75]. It is difficult to place an estimate of the uncertainty in this number due to the limited range of temperature covered in the data and in the fact that only a few lines could be measured in each case. The simulations agree well with the experimental data which would indicate that the estimates placed on n were reasonable. In order to match the reported values at their higher temperatures of the shock tube measurements, a value of 0.44 was used on values of $J'' < 60$. This value is below the "theoretical" value of 0.5 but gave a better representation of the values at a higher temperature. It is not intended to be viewed as a number valid over a large range of temperatures. For higher temperatures the empirical formula #16 reported in Lee, et al. [73] was used. The values at higher temperatures were derived directly from that formula rather than by scaling the values from 296 K.

Our comparison starts from high temperatures (T >1800 K) and low pressures (P <10 kPa), for sharp absorption features and less impact from pressure broadening and shifts. In Fig.9, measured spectra, AI-3000K, UCL-4000 [53], and HITEMP [51] based simulations are plotted by black, green, red, and blue lines, respectively. Nearly all the observed absorption peaks can easily find their counterparts on green and blue lines, with reasonable matches for relative intensity ratio and patterns. The peak-by-peak line

position agreements are mostly within ±0.003 – 0.006 cm^{-1}. Obviously, the experiment based CDSD 2019 energy levels have provided a significant accuracy boost for AI-3000K line positions. Many peak absorptions of AI-3000K (green) and HITEMP (blue) match experimental values within ±10-20%. This supports the reliability of Ames-2021(-40K) DMS and IR intensity calculations. Note the measured absorptions are usually found at higher side in these comparisons at high T and low P.

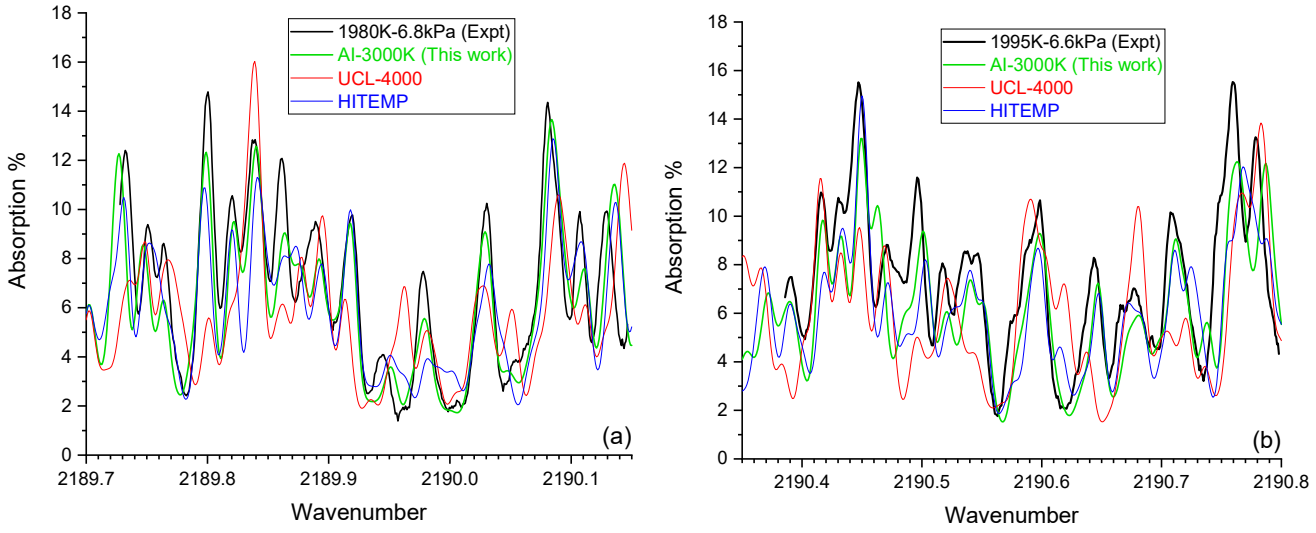

Figure 9. Shock tube IR spectra [72] (black) compared to AI-3000K (green), UCL-4000 (red), and HITEMP (blue). (a) 1980 K, 6.8 kPa, 2189.7 – 2190.15 cm^{-1}; (b) 1995 K, 6.6 kPa, 2190.4 – 2190.8 cm^{-1}.

In Fig.9, the red lines of UCL-4000 [53] generally have larger deviations for both line positions and intensities. Their absorptions can be off by 40% or more at some peak locations, e.g., at 2189.8 cm^{-1}, or at 2190.49 – 2190.55 cm^{-1}. Not all the observed features can be confidently matched to UCL-4000 peaks because both line position and intensity deviations can provide multiple plausible candidates, e.g., at 2189.95 – 2189.98 cm^{-1}, and at 2190.67 – 2190.73 cm^{-1}. Similar observations are noted in additional comparisons. These deficiencies could be partially related to the Ames-1 PES [37] adopted in UCL-4000 rovibrational calculation. The impact of UCL 2015 DMS [40,64] or its implementation in TROVE calculation [77] is unclear for this specific region. Therefore, further comparison and analysis in this section will focus on the thick lines of AI-3000K (green) and HITEMP [51] (blue).

In Fig.9a, the green line of AI-3000K is closer than the blue line of HITEMP [51] to experiment at several major peaks, with exceptions at 2189.95 cm^{-1} and 2190.10 cm^{-1}. Compared to HITEMP, AI-3000K has better agreement for intensity patterns at 2189.75 cm^{-1}, and 2189.96 – 2190.01 cm^{-1}. In Fig.9b, AI-3000K finds better agreement at 2190.42 cm^{-1}, 2190.51 – 2190.54 cm^{-1}, 2190.62 cm^{-1}, and 2190.78 cm^{-1}, while HITEMP has better agreement at 2190.44 cm^{-1} and 2190.47 cm^{-1}. In short, AI-3000K and HITEMP are comparable in the range of Fig.9, and there are more places for AI-3000K to find better agreements with experiment. This observation holds for additional spectra comparison.

However, it is too early to claim the AI-3000K intensity is generally more accurate than HITEMP [51]. First, the shock tube study was limited to a 3 cm^{-1} range in the ν_3 fundamental peak region. A full evaluation will need many more high-resolution experiments in broader wavenumber ranges, as well as wider temperature ranges, e.g., up to 3000 K. Secondly, the uncertainty associated with *some* shock tube experiment data may need case by case evaluation, especially for the pressure (P). According to Mulvihill

and Petersen [72], the general uncertainty estimates were 1.0% for T, 1.8% for P, and 1.5% for absorption detection and emission. But its Fig.5 has a $T = 1910 \pm 70$ K, i.e., a 3.6% uncertainty for temperature. Its Fig.6 has a $P = 7.5 \pm 1.4$ kPa, i.e., a 19% uncertainty for pressure. Pressure is proportional to the number of molecules in the optical path, and the simulated absorption strengths. Pressure deviations will inevitably cause deviations on the simulated spectra. Technically, the P and T uncertainties combined can easily exceed the peak difference between AI-3000K and HITEMP absorptions. As Ref. [72] did not report individual P/T uncertainties for the bulk of shock tube spectra, more inclusive and semi quantitative analysis will be necessary before making accuracy claims beyond 10-20%.

From our limited comparisons of ~20 spectra, the overall relative uncertainty was estimated to be 6±3%, averaged for the shock tube spectra dataset reported in Ref. [72]. It would be ideal if those spectra carrying unexpectedly large uncertainties can be identified, or individual P and T uncertainties can be determined. Although it is beyond the scope of this study, the quality and consistency of and between AI-3000K and HITEMP [51] can provide insights on the topic. An example at 2189 cm^{-1} is given in Fig.10 and Fig.11.

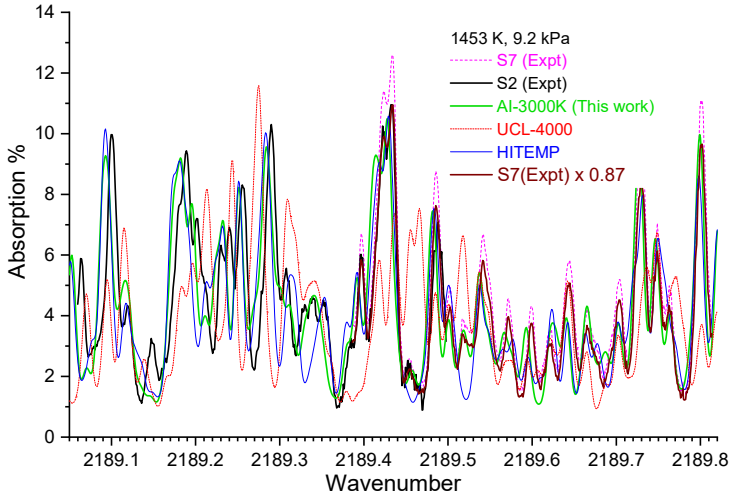

Figure 10. Shock tube IR spectra [72] (Expt, S2 – black, S7 – dashed magenta, S7 scaled – brown) compared to AI-3000K (green), UCL-4000 [53] (dashed red), and HITEMP [51] (blue) based simulations. The S2 spectra covers 2189.06 – 2189.49 cm^{-1}. The S7 (and S7 scaled) spectra covers 2189.38 – 2189.81 cm^{-1}. Both S2 and S7 were reported at 1453 K and 9.2 kPa.

The S2 and S7 spectra in the supplementary file of Ref. [72] were both reported at 1453 K and 9.2 kPa. They overlap with each other from 2189.38 cm^{-1} to 2189.49 cm^{-1}, but their peak absorptions diverge by more than 10%. As shown in Fig.10, the AI-3000K (green) and HITEMP [51] (blue) peak absorptions are in good agreement with S2 spectra (solid black) on the left, but visibly weaker than S7 spectra (dashed magenta) on the right. If the S7 spectra is scaled by 0.87 to match the S2 spectra in the overlapped range (see the solid brown line), the experiment vs AI-3000K / HITEMP agreement is brought back to the level of S2 spectra, as shown in Fig.10. Are these agreements accidental?

In order to get a more reliable answer or estimate, we run additional comparisons focusing on the peak at 2189.43 cm^{-1}, i.e., the peak at the center of Fig.10. In Fig.11a, 7 experiment spectra are compared to six AI-3000K based simulations. Two experiment spectra, S6 and S7, are plotted as dashed orange and magenta lines, because they appear inconsistent with other experiment spectra. From A to F, the reported peak absorptions are higher than those of AI-3000K by 21%, 12%, 4% (or 20%), 15%, 37%, and 40%, respectively. The S6 (F) spectra has the largest intensity difference, an unusual position red-shift, and absorptions higher than D and close to C (S2).

Fig.11b demonstrates the consistency between AI-3000K and HITEMP [51] in the same narrow range of 0.08 cm^{-1}. From A to F, peak absorptions of HITEMP (blue) are higher than those of AI-3000K (green) by 1.5%, 1.2%, 0.7%, 0.3%, -0.5%, and 1.0%, respectively. This means the impact of *P*:*T* condition changes are mostly systematic on intensities, and they are highly consistent between AI-3000K and HITEMP. Now the S6 (*F*) spectra in Fig.11a can be safely identified as an outlier. Nevertheless rest A-E spectra and simulations follow similar intensity ladder in both Fig.11*a* and Fig.11*b* panels, with different separations among spectra though. It is still not 100% clear if the differences in Fig.11a are mainly resulted from unknown deficiencies of AI-3000K (and HITEMP), or from the underestimation of pressure in the shock tube experiments (so S7 is an outlier), or both. Note it is highly unlikely to attribute the intensity differences to line position deviations in AI-3000K or HITEMP that potentially become larger at higher *J* and higher vibrational quanta, or energy.

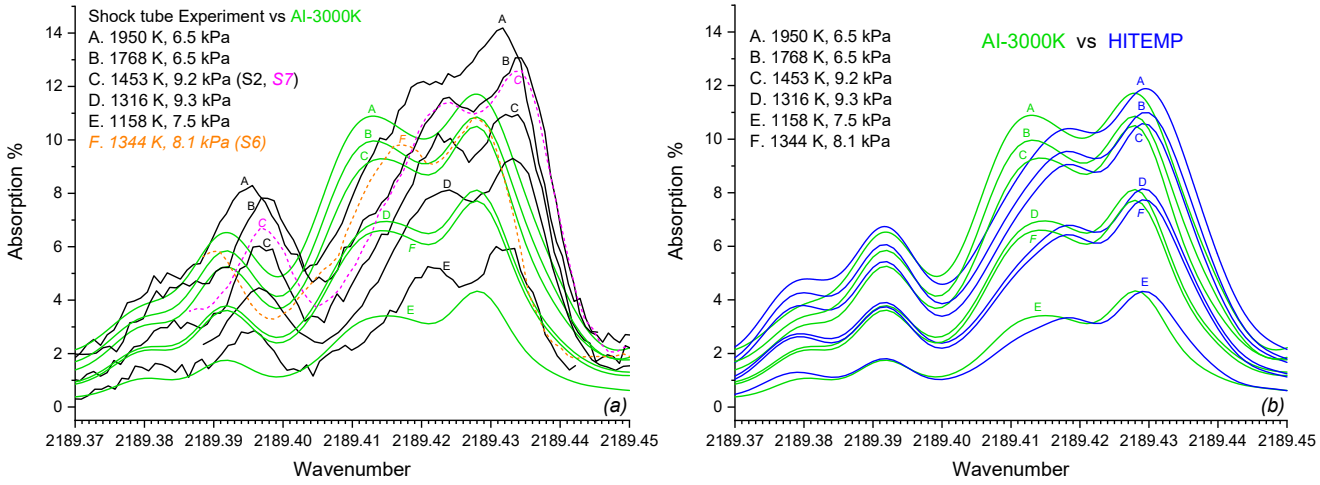

Figure 11. Compare the shock tube experiment [72] and IR simulations at 6 reported pressures and temperatures, numbered from A to F. a) experiment (black lines, or dashed orange line for S6, and dashed magenta line for S7) vs AI-3000K (green); b) AI-3000K (green) vs HITEMP [51](blue).

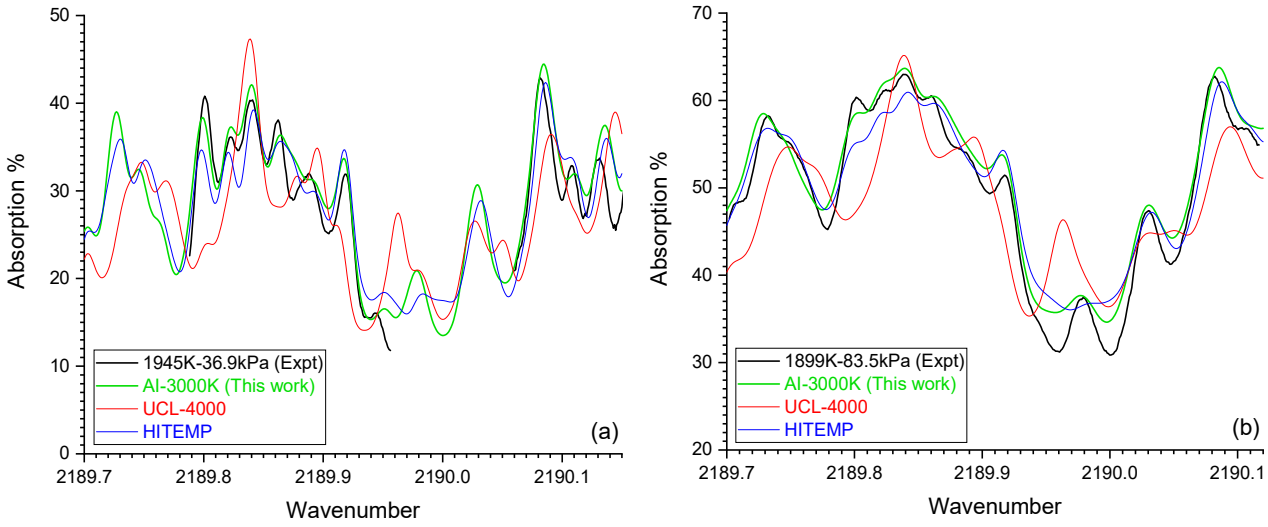

Figure 12. Shock tube IR spectra [72] (black) compared to AI-3000K (green), UCL-4000 [53] (red), and HITEMP [51] (blue), between 2189.7 – 2190.15 cm^{-1}. (a) 1945 K, 36.9 kPa; (b) 1899 K, 83.5 kPa.

The intensity predictions of HITEMP [51] and AI-3000K are based upon two totally different schemes: experimental Effective Hamiltonian and dipole models, or quantum rovibrational calculations using high level *ab initio* PES and DMS. They were expected to have reliable intensity predictions and reasonable agreement with experiments. Now their peak intensities are more consistent with each other than with experiment. Remember that the Fig.7 in Section IV has a quantitative estimate for the intensity convergence of AI-3000K line list. Around 2189 cm^{-1}, the $\Delta S/S_{40K}$ ratio is less than 10^{-7} at 2000 K, or less than 5×10^{-5} at 3000 K, or less than 5×10^{-4} (or 0.05%) at 4000 K. In other words, this spectra range is extraordinarily stable. Contributions from PES or DMS higher energy region (e.g., thousands of hot bands) only have minimal impact. The reliability of AI-3000K prediction in this range would be much higher than those discussed for general scenarios in Section IV. Therefore, the AI-3000K and HITEMP are not expected to have systematic intensity deviations > 10% at 2000 K. However, we must be prepared to look for unknown factors contributing to such deviations, in case they are confirmed by future studies.

The intensity discrepancy at higher pressure has also been checked. Fig.12 compares absorptions in the same range of Fig.9a, i.e., 2189.7 – 2190.1 cm^{-1}, with similar temperature but pressure increased from 6.8 kPa to 36.9 kPa in panel *a*, and 83.5 kPa in panel *b*. As expected, higher pressure leads to less sharp features. The 15 absorption peaks in Fig.9a have merged into 4-5 wider bumps in Fig.12b. Compared to HITEMP [51] (blue) lines, the AI-3000K (green) lines are stronger and closer to experiment (black) lines. These are consistent with Fig.9a, while the peak absorptions of AI-3000K and HITEMP now have better agreement with shock tube spectra in both panels of Fig.12.

Additional comparison suggests that the agreement level between AI-3000K and experiment could be related to pressure. It is noticed that the agreement varies from ~10% underestimation below 10 kPa, to being roughly similar in the range of 10 – 20 kPa, then to minor overestimation at higher pressure. Note this observation still needs independent verification, but here are the potentially contributing factors (if confirmed): (1) the uncertainty of *P* remains about the same, so the relative uncertainty of *P* was significantly reduced at higher pressure; (2) the line shape model for 2000 K simulation of CO_2-Ar system needs enhancement to improve the agreement with measured spectra; (3) the *P* estimate in shock tube experiment had minor underestimation.

On the other hand, the troughs of both AI-3000K and HITEMP [51] simulations in Fig.12b are explicitly stronger than those measured at 2189.78 cm^{-1}, 2189.90 cm^{-1}, 2189.96 cm^{-1}, 2190.00 cm^{-1}, and 2190.05 cm^{-1}. Assuming the *P* and *T* uncertainty had been minimized and the broadening model is reliable, one potential explanation is that the AI-3000K and HITEMP line lists contain weak lines carrying overestimated or fake intensity. They could have boosted the whole spectra to *accidentally* agree with experiment peak heights, but unavoidably appearing stronger at the bottom of troughs. This sounds plausible but there is not enough evidence for or against it, so will be another focus of future investigation.

It should be noted that the differences between HITEMP based simulations and CDSD-4000 based simulations are negligible or very small at the Shock Tube experiment conditions up to 2000 K, especially when they are compared to the database and experiment differences shown in Figs.9-12. In other words, they can be considered equivalent, so CDSD-4000 is not explicitly compared in this section.

VI. Summary and Future Improvements

The construction of AI-3000K IR line list is introduced, including the generation and quality of a new dipole moment surface (Ames-2021-40K) accurately fitted up to 40,000 cm^{-1}, and a new potential energy surface (X01d) refined with respect to selected CDSD2019 [45] levels. The line list computations cover the range of 0 – 20,000 cm^{-1} for the 4 most abundant isotopologues: 626, 636, 628 and 627. The J=0-150 CDSD energy levels up to 24,000 cm^{-1} are adopted to upgrade the corresponding X01d PES based line positions, and A_{21} coefficients of Ames-2021 296 K IR line lists [60] are utilized to replace their counterparts for transitions with $E' < 15{,}000$ cm^{-1}. In short, the AI-3000K line list is the CDSD oriented X01d PES and Ames-2021-40K DMS based line list enhanced with the Ames-2 PES and Ames-2021 DMS based A_{21} coefficients, and CDSD energy levels..

In total, AI-3000K has 36 billion IR transitions, and its compact storage occupies 400 GB. Convergence tests and analysis are carried out for isotopologues, upper state energy E' cutoff, and lower state energy E'' cutoff. The AI-3000K line list is converged to better than 90% for 0 – 20,000 cm^{-1} at 1000 K, or 0 – 15,000 cm^{-1} at 2000 K, and 0 – 9000 cm^{-1} at 3000 K. Convergence for 4000 K and above will require new PES and new DMS effectively covering the region of $E' > 40000$ cm^{-1}. Because the UCL-4000 [53] line list had intensity noises above 10,000 cm^{-1}, and missed some intensities below 10,000 cm^{-1} due to the $E''<16{,}000$ cm^{-1} cutoff, AI-3000K provides a better candidate for hot CO_2 IR analysis and simulation up to 3000 K. Please note experimental intensities or experiment based effective dipole model (e.g., CDSD) predictions are still recommended for transitions or bands strongly perturbed by Coriolis interactions [60].

The comparisons with shock tube IR spectra near 2000 K demonstrate that AI-3000K line list carries line position accuracy analogous to HITEMP [51], and better intensity agreement at more places. In other words, the new algorithm adopted in AI-3000K construction seems to be working satisfactorily. The CDSD energy levels have provided critical boost for line position accuracy of AI-3000K. The quality of the CDSD oriented X01d PES, Ames-2021-40K DMS and Ames-2021 IR line lists have passed first round of tests. Questions remain about some discrepancies observed at different temperatures or pressures. Finding answers or solutions to those questions will rely on the future synergy between experiment and theory.

From a perspective of semi-empirical IR line list calculations, it seems not immediately practicable to refine PES or evaluate DMS with respect to the experimentally measured absorptions. This is mainly due to the uncertainties discussed in Section V. We hope the AI-3000K list will be independently evaluated by colleague groups, and compared to more high-resolution experiments when available. Hopefully, future experiments at different pressures and higher temperatures will offer more insights and help elucidate the agreement changes associated with pressure. IR intensity reliably measured at high temperature in stable regions (e.g., absorption peaks of major vibrational bands) may help enhance the intensity accuracy of semi-empirical IR line list for some important hot bands that are not too weak at room temperature. From the interest of line list convergence, high-resolution experiments are desperately needed for those sensitive regions as discussed in Section IV.2 and IV.3, e.g., 1700 – 1900 cm^{-1}, and 2650 – 2850 cm^{-1}. Absorptions in those regions will be far more challenging for semi-empirical IR line lists to predict reliably, or accurately.

In Figs. 9-12, part of the differences between AI-3000K and HITEMP2010 are caused by the upgrade of CDSD models from 2010 to 2019, and AI-3000K uses the 2019 CDSD levels which we assume

more reliable. On the other hand, the line position differences with respect to measured spectra should be investigated in future, because pressure shifts are not incorporated in Section V simulations. But existing pressure shift parameters are based on lower temperature experiments, not necessarily suitable for 2000 – 4000 K analysis. The line position deviations in Figs. 9-12 are obviously dependent upon specific peak or band. It requires more detailed analysis to check the major transitions or bands behind an absorption peak, and to estimate the impact of pressure shift which has been corrected to 2000 K. If the impact is not large enough to cause 0.003 – 0.006 cm^{-1} shifts, it may be necessary to consider the accuracy loss of CDSD energy levels at high energy and high J's. This path potentially leads to more accurate PES refinement, which accordingly will help generate more reliable IR line lists, e.g., Ames-4000K in future. It may be also necessary for PES refinements to include higher order terms to improve the accuracy at high energy or high J.

Acknowledgement

We gratefully acknowledge support from the NASA Grants 17-APRA17-0051, 18-APRA18-0013 and 18-XRP18_2-0029. X.H. acknowledges the support by NASA/SETI Institute Co-operative Agreements NNX17AL03G, 80NSSC19M0121 and 80NSSC20K1358. R.F. acknowledges the support from NASA/SETI Institute Co-operative Agreement 80NSSC19K1036. S.T. acknowledges support from the Ministry of Science and Higher Education of the Russian Federation. We thank Dr. Hargreaves and Dr. Gordon (Harvard CfA, HITRAN) for stimulating comments and helpful discussions. Resources supporting this work were provided by the NASA High-End Computing (HEC) Program through the NASA Advanced Supercomputing (NAS) Division at Ames Research Center.

Dr. Timothy J. Lee tragically passed away on November 3, during the course of this work. It was of high importance to him to contribute to the Festschrift for Professor Per Jensen, whose scientific achievements have greatly inspired generations of colleagues in the spectroscopy field. The remaining authors would therefore like this work to be recognized to honor two highly merited scientists: Professor Per Jensen and Dr. Timothy J. Lee.

Supplementary materials:

The supplementary data files associated with this article include: The supplementary files are:

(1) a README file for AI-3000K line list calculation and additional statistics.

(2) CO_2 X01d PES subroutine and coefficients (also available from http://huang.seti.org), input and output of X01d PES refinement.

(3) Ames-2021-40K DMS subroutine and coefficients (also available from http://huang.seti.org), fitting deviations on 11155 geometries.

(4) an ORIGIN project file containing the figures and data analysis presented in this paper. Please use Origin Viewer (www.originlab.com/viewer) to open and extract data.

(5) a FORTRAN program to convert the .tgz files back into simple text format, and a readme for convert.f90 file to explain how to use and customize the program to generate hot CO_2 line list at user specified temperature and with flexible format.

(6)* Rovibrational energy level lists for 4 CO_2 isotopologues, and a list of zero point energy and partition function values at 296 K, 1000 K, 2000 K, 3000 K, and 4000 K. (~530 MB in .tgz format)

(7)* 2000 .tgz files of AI-3000K IR line list, covering 0 – 20,000 cm^{-1}. (~400 GB)

Files #(1) - #(5) are published with this article at https://doi.org/10.1016/j.jmspec.2023.xxx (to be updated at proof stage). Because the size of files #(6) and #(7) exceed the maximum data size allowed by journal, they are being released together with other files through the dataset portal of NASA Advanced Supercomputing Division at https://data.nas.nasa.gov/ai3000k, which will be freely available to public.

References

---

[1] F. Oyafuso, V.H. Payne, B.J. Drouin, V.M. Devi, D.C. Benner, K. Sung, S. Yu, I.E. Gordon, R. Kochanov, Y. Tan, D. Crisp, E.J. Mlawer, A. Guillaume, High accuracy absorption coefficients for the Orbiting Carbon Observatory-2 (OCO-2) mission: Validation of updated carbon dioxide cross-sections using atmospheric spectra, J. Quant. Spectrosc. Radiat. Transf. 203 (2017) 213–223. https://doi.org/10.1016/j.jqsrt.2017.06.012.

[2] A. Fedorova, B. Bézard, J.L. Bertaux, O. Korablev, C. Wilson, The CO_2 continuum absorption in the 1.10- and 1.18-μm windows on Venus from Maxwell Montes transits by SPICAV IR onboard Venus express, Planet. Space Sci. 113–114 (2015) 66–77. https://doi.org/10.1016/j.pss.2014.08.010.

[3] C.R. Webster, P.R. Mahaffy, G.J. Flesch, P.B. Niles, J.H. Jones, L.A. Leshin, S.K. Atreya, J.C. Stern, L.E. Christensen, T. Owen, H. Franz, R.O. Pepin, A. Steele, Isotope Ratios of H, C, and O in CO_2 and H_2O of the Martian Atmosphere, Science 341 (2013) 260–263. https://doi.org/10.1126/science.1237961.

[4] G.M. Shved, On the abundances of carbon dioxide isotopologues in the atmospheres of mars and earth, Sol. Syst. Res. 50 (2016) 161–164. https://doi.org/10.1134/s0038094616020064.

[5] V.G. Kunde, Jupiter's Atmospheric Composition from the Cassini Thermal Infrared Spectroscopy Experiment, Science 305 (2004) 1582–1586. https://doi.org/10.1126/science.1100240.

[6] T. deGraauw, H. Feuchtgruber, B. Bezard, P. Drossart, T. Encrenaz, D. Beintema, M. Griffin, A. Heras, M. Kessler, K. Leech, E. Lellouch, P. Morris, P. Roelfsema, M. RoosSerote, A. Salama, B. Vandenbussche, E. Valentijn, G. Davis, D. Naylor, First results of ISO-SWS observations of Saturn: Detection of CO_2, CH_3C_2H, C_4H_2 and tropospheric H_2O, Astron. Astrophys. 321 (1997) L13.

[7] H. Feuchtgruber, E. Lellouch, T. de Graauw, B. Bézard, T. Encrenaz, M. Griffin, External supply of oxygen to the atmospheres of the giant planets, Nature 389 (1997) 159–162. https://doi.org/10.1038/38236.

[8] R.E. Samuelson, W.C. Maguire, R.A. Hanel, V.G. Kunde, D.E. Jennings, Y.L. Yung, A.C. Aikin, CO_2 on Titan, J. Geophys. Res. Sp. Phys. 88 (1983) 8709–8715. https://doi.org/10.1029/JA088iA11p08709.

[9] S.M. Hörst, Titan's atmosphere and climate, J. Geophys. Res. Planets. 122 (2017) 432–482. https://doi.org/10.1002/2016JE005240.

[10] R.W. Carlson, A Tenuous Carbon Dioxide Atmosphere on Jupiter's Moon Callisto, Science 283 (1999) 820–821. https://doi.org/10.1126/science.283.5403.820.

[11] C.A. Hibbitts, T.B. McCord, G.B. Hansen, Distributions of CO_2 and SO_2 on the surface of Callisto, J. Geophys. Res. Planets. 105 (2000) 22541–22557. https://doi.org/10.1029/1999JE001101.

[12] R.H. Brown, Composition and Physical Properties of Enceladus' Surface, Science 311 (2006) 1425–1428. https://doi.org/10.1126/science.1121031.

[13] T. Ootsubo, H. Kawakita, S. Hamada, H. Kobayashi, M. Yamaguchi, F. Usui, T. Nakagawa, M. Ueno, M. Ishiguro, T. Sekiguchi, J.I. Watanabe, I. Sakon, T. Shimonishi, T. Onaka, AKARI near-infrared spectroscopic survey for CO_2 in 18 comets, Astrophys. J. 752 (2012). https://doi.org/10.1088/0004-637X/752/1/15.

[14] D. Bockelée-Morvan, U. Calmonte, S. Charnley, J. Duprat, C. Engrand, A. Gicquel, M. Hässig, E. Jehin, H. Kawakita, B. Marty, S. Milam, A. Morse, P. Rousselot, S. Sheridan, E. Wirström, Cometary Isotopic Measurements, Space Sci. Rev. 197 (2015) 47–83. https://doi.org/10.1007/s11214-015-0156-9.

[15] M.R. Line, M.S. Marley, M.C. Liu, B. Burningham, C. V. Morley, N.R. Hinkel, J. Teske, J.J. Fortney, R.

Lupu, R. Freedman, Uniform Atmospheric Retrieval Analysis of Ultracool Dwarfs II: Properties of 11 T-dwarfs, Astrophys. J. 848 (2016) 83. https://doi.org/10.3847/1538-4357/aa7ff0.

[16] R.S. Freedman, J. Lustig-Yaeger, J.J. Fortney, R.E. Lupu, M.S. Marley, K. Lodders, Gaseous mean opacities for giant planet and ultracool dwarf atmospheres over a range of metalicities and temperatures Astrophys. J. Suppl. Ser. 214 (2014) 25. https://doi.org/10.1088/0067-0049/214/2/25.

[17] B.R. Oppenheimer, C. Baranec, C. Beichman, D. Brenner, R. Burruss, E. Cady, J.R. Crepp, R. Dekany, R. Fergus, D. Hale, L. Hillenbrand, S. Hinkley, D.W. Hogg, D. King, E.R. Ligon, T. Lockhart, R. Nilsson, I.R. Parry, L. Pueyo, E. Rice, J.E. Roberts, L.C. Roberts, M. Shao, A. Sivaramakrishnan, R. Soummer, T. Truong, G. Vasisht, A. Veicht, F. Vescelus, J.K. Wallace, C. Zhai, N. Zimmerman, Reconnaissance of the HR 8799 exosolar system. I. Near-Infrared Spectroscopy, Astrophys. J. 768 (2013) 24. https://doi.org/10.1088/0004-637X/768/1/24.

[18] M.R. Swain, G. Tinetti, G. Vasisht, P. Deroo, C. Griffith, J. Bouwman, P. Chen, Y. Yung, A. Burrows, L.R. Brown, J. Matthews, J.F. Rowe, R. Kuschnig, D. Angerhausen, Water, Methane, and Carbon Dioxide present in the dayside spectrum of the exoplanet HD 209458b, Astrophys. J. 704 (2009) 1616–1621. https://doi.org/10.1088/0004-637X/704/2/1616.

[19] M.R. Swain, P. Deroo, C.A. Griffith, G. Tinetti, A. Thatte, G. Vasisht, P. Chen, J. Bouwman, I.J. Crossfield, D. Angerhausen, C. Afonso, T. Henning, A ground-based near-infrared emission spectrum of the exoplanet HD 189733b, Nature 463 (2010) 637–639. https://doi.org/10.1038/nature08775.

[20] A.S. Burrows, Highlights in the study of exoplanet atmospheres, Nature 513 (2014) 345–352. https://doi.org/10.1038/nature13782.

[21] K. Heng, J.R. Lyons, Carbon Dioxide in Exoplanetary Atmospheres: Rarely Dominant Compared to Carbon Monoxide and Water in Hot, Hydrogen-dominated Atmospheres, Astrophys. J. 817 (2015) 149. https://doi.org/10.3847/0004-637X/817/2/149.

[22] P. Gao, R. Hu, T.D. Robinson, C. Li, Y.L. Yung, Stability of CO_2 Atmospheres on Desiccated M Dwarf Exoplanets, Astrophys. J. 806 (2015) 249. https://doi.org/10.1088/0004-637X/806/2/249.

[23] E. Marcq, F.P. Mills, C.D. Parkinson, A.C. Vandaele, Composition and Chemistry of the Neutral Atmosphere of Venus, Space Sci. Rev. 214 (2018). https://doi.org/10.1007/s11214-017-0438-5.

[24] J.B. Pollack, J.B. Dalton, D. Grinspoon, R.B. Wattson, R. Freedman, D. Crisp, D.A. Allen, B. Bezard, C. DeBergh, L.P. Giver, Q. Ma, R. Tipping, Near-Infrared Light from Venus' Nightside: A Spectroscopic Analysis, Icarus 103 (1993) 1–42. https://doi.org/10.1006/icar.1993.1055.

[25] J.I. Moses, N. Madhusudhan, C. Visscher, R.S. Freedman, Chemical consequences of the C/O ratio on hot jupiters: Examples from WASP-12b, CoRoT-2b, XO-1b, and HD 189733b, Astrophys. J. 763 (2013). https://doi.org/10.1088/0004-637X/763/1/25.

[26] H. Massol, K. Hamano, F. Tian, M. Ikoma, Y. Abe, E. Chassefière, A. Davaille, H. Genda, M. Güdel, Y. Hori, F. Leblanc, E. Marcq, P. Sarda, V.I. Shematovich, A. Stökl, H. Lammer, Formation and Evolution of Protoatmospheres, Space Sci. Rev. 205 (2016) 153–211. https://doi.org/10.1007/s11214-016-0280-1.

[27] P.A. Sabelhaus, J.E. Decker, An overview of the James Webb Space Telescope (JWST) project, in: J.C. Mather (Ed.), 2004: p. 550. https://doi.org/10.1117/12.549895.

[28] T.P. Greene, M.R. Line, C. Montero, J.J. Fortney, J. Lustig-Yaeger, K. Luther, Characterizing transiting exoplanet atmospheres with JWST, Astrophys. J. 817 (2016) 17. https://doi.org/10.3847/0004-637X/817/1/17.

[29] B. Edwards, L. Mugnai, G. Tinetti, E. Pascale, S. Sarkar, An Updated Study of Potential Targets for Ariel, Astron. J. 157 (2019) 242. https://doi.org/10.3847/1538-3881/ab1cb9.

[30] D. Spergel, N. Gehrels, C. Baltay, D. Bennett, J. Breckinridge, M. Donahue, A. Dressler, B.S. Gaudi, T.

Greene, O. Guyon, C. Hirata, J. Kalirai, N.J. Kasdin, B. Macintosh, W. Moos, S. Perlmutter, M. Postman, B. Rauscher, J. Rhodes, Y. Wang, D. Weinberg, D. Benford, M. Hudson, W.-S. Jeong, Y. Mellier, W. Traub, T. Yamada, P. Capak, J. Colbert, D. Masters, M. Penny, D. Savransky, D. Stern, N. Zimmerman, R. Barry, L. Bartusek, K. Carpenter, E. Cheng, D. Content, F. Dekens, R. Demers, K. Grady, C. Jackson, G. Kuan, J. Kruk, M. Melton, B. Nemati, B. Parvin, I. Poberezhskiy, C. Peddie, J. Ruffa, J.K. Wallace, A. Whipple, E. Wollack, F. Zhao, Wide-Field InfrarRed Survey Telescope-Astrophysics Focused Telescope Assets WFIRST-AFTA 2015 Report, Control. (2015). http://arxiv.org/abs/1503.03757.

[31] The LUVOIR Team, The LUVOIR Mission Concept Study Final Report, (2019). http://arxiv.org/abs/1912.06219.

[32] B. Bézard, A. Fedorova, J.L. Bertaux, A. Rodin, O. Korablev, The 1.10- and 1.18-μm nightside windows of Venus observed by SPICAV-IR aboard Venus Express, Icarus 216 (2011) 173–183. https://doi.org/10.1016/j.icarus.2011.08.025.

[33] P. Tremblin, D.S. Amundsen, P. Mourier, I. Baraffe, G. Chabrier, B. Drummond, D. Homeier, O. Venot, Fingering convection and cloudless models for cool brown dwarf atmospheres, Astrophys. J. Lett. 804 (2015) 6. https://doi.org/10.1088/2041-8205/804/1/L17.

[34] R.S. Freedman, M.S. Marley, K. Lodders, Line and Mean Opacities for Ultracool Dwarfs and Extrasolar Planets, Astrophys. J. Suppl. Ser. 174 (2008) 504–513. https://doi.org/10.1086/521793.

[35] J.K. Barstow, C.C.C. Tsang, C.F. Wilson, P.G.J. Irwin, F.W. Taylor, K. McGouldrick, P. Drossart, G. Piccioni, S. Tellmann, Models of the global cloud structure on Venus derived from Venus Express observations, Icarus 217 (2012) 542–560. https://doi.org/10.1016/j.icarus.2011.05.018.

[36] B. Fleury, M.S. Gudipati, B.L. Henderson, M. Swain, Photochemistry in Hot H_2-dominated Exoplanet Atmospheres, Astrophys. J. 871 (2019) 158. https://doi.org/10.3847/1538-4357/aaf79f.

[37] X. Huang, D.W. Schwenke, S.A. Tashkun, T.J. Lee, An isotopic-independent highly accurate potential energy surface for CO_2 isotopologues and an initial $^{12}C^{16}O_2$ infrared line list, J. Chem. Phys. 136 (2012) 124311. https://doi.org/10.1063/1.3697540.

[38] X. Huang (黄新川), R.R. Gamache, R.S. Freedman, D.W. Schwenke, T.J. Lee, *Reliable infrared line lists for 13 CO_2 isotopologues up to E'=18,000 cm^{-1} and 1500 K, with line shape parameters*, J. Quant. Spectrosc. Radiat. Transf. 147 (2014) 134–144. https://doi.org/10.1016/j.jqsrt.2014.05.015.

[39] S.A. Tashkun, V.I. Perevalov, R.R. Gamache, J. Lamouroux, CDSD-296, high resolution carbon dioxide spectroscopic databank: Version for atmospheric applications, J. Quant. Spectrosc. Radiat. Transf. 152 (2015) 45–73. https://doi.org/10.1016/j.jqsrt.2014.10.017.

[40] E. Zak, J. Tennyson, O.L. Polyansky, L. Lodi, N.F. Zobov, S.A. Tashkun, V.I. Perevalov, A room temperature CO_2 line list with ab initio computed intensities, J. Quant. Spectrosc. Radiat. Transf. 177 (2015) 1–12. https://doi.org/10.1016/j.jqsrt.2015.12.022.

[41] E.J. Zak, J. Tennyson, O.L. Polyansky, L. Lodi, N.F. Zobov, S.A. Tashkun, V.I. Perevalov, Room temperature line lists for CO_2 symmetric isotopologues with ab initio computed intensities, J. Quant. Spectrosc. Radiat. Transf. 189 (2017) 267–280. https://doi.org/10.1016/j.jqsrt.2016.11.022.

[42] E.J. Zak, J. Tennyson, O.L. Polyansky, L. Lodi, N.F. Zobov, S.A. Tashkun, V.I. Perevalov, Room temperature linelists for CO_2 asymmetric isotopologues with ab initio computed intensities, J. Quant. Spectrosc. Radiat. Transf. 203 (2017) 265–281. https://doi.org/10.1016/j.jqsrt.2017.01.037.

[43] X. Huang (黄新川), D.W. Schwenke, R.S. Freedman, T.J. Lee, *Ames-2016 line lists for 13 isotopologues of CO_2 : Updates, consistency, and remaining issues*, J. Quant. Spectrosc. Radiat. Transf. 203 (2017) 224–241. https://doi.org/10.1016/j.jqsrt.2017.04.026.

[44] I.E. Gordon, L.S. Rothman, C. Hill, R.V. Kochanov, Y. Tan, P.F. Bernath, M. Birk, V. Boudon, A.

Campargue, K.V. Chance, B.J. Drouin, J.-M. Flaud, R.R. Gamache, J.T. Hodges, D. Jacquemart, V.I. Perevalov, A. Perrin, K.P. Shine, M.-A.H. Smith, J. Tennyson, G.C. Toon, H. Tran, V.G. Tyuterev, A. Barbe, A.G. Császár, V.M. Devi, T. Furtenbacher, J.J. Harrison, J.-M. Hartmann, A. Jolly, T.J. Johnson, T. Karman, I. Kleiner, A.A. Kyuberis, J. Loos, O.M. Lyulin, S.T. Massie, S.N. Mikhailenko, N. Moazzen-Ahmadi, H.S.P. Müller, O.V. Naumenko, A.V. Nikitin, O.L. Polyansky, M. Rey, M. Rotger, S.W. Sharpe, K. Sung, E. Starikova, S.A. Tashkun, J. Vander Auwera, G. Wagner, J. Wilzewski, P. Wcisło, S. Yu, E.J. Zak, *The HITRAN2016 molecular spectroscopic database*, J. Quant. Spectrosc. Radiat. Transf. 203 (2017) 3–69. https://doi.org/10.1016/j.jqsrt.2017.06.038.

[45] S.A. Tashkun, V.I. Perevalov, R.R. Gamache, J. Lamouroux, CDSD-296, high-resolution carbon dioxide spectroscopic databank: An update, J. Quant. Spectrosc. Radiat. Transf. 228 (2019) 124–131. https://doi.org/10.1016/j.jqsrt.2019.03.001.

[46] E.V. Karlovets, I.E. Gordon, L.S. Rothman, R. Hashemi, R.J. Hargreaves, G.C. Toon, A. Campargue, V.I. Perevalov, P. Čermák, M. Birk, G. Wagner, J.T. Hodges, J. Tennyson, S.N. Yurchenko, The update of the line positions and intensities in the line list of carbon dioxide for the HITRAN2020 spectroscopic database, J. Quant. Spectrosc. Radiat. Transf. 276 (2021) 107896. https://doi.org/10.1016/j.jqsrt.2021.107896.

[47] R.B. Wattson, L.S. Rothman, Determination of vibrational energy levels and parallel band intensities of $^{12}C^{16}O_2$ by Direct Numerical Diagonalization, J. Mol. Spectrosc. 119 (1986) 83–100. https://doi.org/10.1016/0022-2852(86)90203-1.

[48] R.B. Wattson, L.S. Rothman, Direct numerical diagonalization: Wave of the future, J. Quant. Spectrosc. Radiat. Transf. 48 (1992) 763–780. https://doi.org/10.1016/0022-4073(92)90140-Y.

[49] S.A. Tashkun, V.I. Perevalov, J.-L. Teffo, A.D. Bykov, N.N. Lavrentieva, CDSD-1000, the high-temperature carbon dioxide spectroscopic databank, J. Quant. Spectrosc. Radiat. Transf. 82 (2003) 165–196. https://doi.org/10.1016/S0022-4073(03)00152-3.

[50] S.A. Tashkun, V.I. Perevalov, CDSD-4000: High-resolution, high-temperature carbon dioxide spectroscopic databank, J. Quant. Spectrosc. Radiat. Transf. 112 (2011) 1403–1410. https://doi.org/10.1016/j.jqsrt.2011.03.005.

[51] L.S. Rothman, I.E. Gordon, R.J. Barber, H. Dothe, R.R. Gamache, A. Goldman, V.I. Perevalov, S.A. Tashkun, J. Tennyson, HITEMP, the high-temperature molecular spectroscopic database, J. Quant. Spectrosc. Radiat. Transf. 111 (2010) 2139–2150. https://doi.org/10.1016/j.jqsrt.2010.05.001.

[52] X. Huang, R.S. Freedman, S.A. Tashkun, D.W. Schwenke, T.J. Lee, Semi-empirical $^{12}C^{16}O_2$ IR line lists for simulations up to 1500K and 20,000 cm^{-1}, J. Quant. Spectrosc. Radiat. Transf. 130 (2013) 134–146. https://doi.org/10.1016/j.jqsrt.2013.05.018.

[53] S.N. Yurchenko, T.M. Mellor, R.S. Freedman, J. Tennyson, ExoMol line lists – XXXIX. Ro-vibrational molecular line list for CO_2, Mon. Not. R. Astron. Soc. 496 (2020) 5282–5291. https://doi.org/10.1093/mnras/staa1874.

[54] I. Suzuki, Anharmonic Potential Functions of Simple Molecules. II. Direct Numerical Diagonalization of Vibratinal Hamiltonian Matrix and Its Application to CO_2 and CS_2, Bull. Chem. Soc. Jpn. 48 (1975) 3565–3572. https://doi.org/10.1246/bcsj.48.3565.

[55] R.J. Whitehead, N.C. Handy, Variational calculation of vibration-rotation energy levels for triatomic molecules, J. Mol. Spectrosc. 55 (1975) 356–373. https://doi.org/10.1016/0022-2852(75)90274-X.

[56] M.P. Esplin, R.B. Wattson, M.L. Hoke, R.L. Hawkins, L.S. Rothman, Observation and calculation of carbon dioxide bands with high vibrational angular momentum, Appl. Opt. 28 (1989) 409. https://doi.org/10.1364/AO.28.000409.

[57] J.L. Teffo, O.N. Sulakshina, V.I. Perevalov, Effective Hamiltonian for rovibrational energies and line

intensities of carbon dioxide, J. Mol. Spectrosc. 156 (1992) 48–64. https://doi.org/10.1016/0022-2852(92)90092-3.

[58] S.A. Tashkun, V.I. Perevalov, J.L. Teffo, V.I.G. Tyuterev, Global fit of $^{12}C^{16}O_2$ vibrational-rotational line intensities using the effective operator approach, J. Quant. Spectrosc. Radiat. Transf. 62 (1999) 571–598. https://doi.org/10.1016/S0022-4073(98)00138-1.

[59] V.I. Perevalov, E.I. Lobodenko, O.M. Lyulin, J.L. Teffo, Effective Dipole Moment and Band Intensities Problem for Carbon Dioxide, J. Mol. Spectrosc. 171 (1995) 435–452. https://doi.org/10.1006/jmsp.1995.1131.

[60] X. Huang, D.W. Schwenke, R.S. Freedman, T.J. Lee, Ames-2021 CO_2 Dipole Moment Surface and IR Line Lists: Toward 0.1% Uncertainty for CO_2 IR Intensities, J. Phys. Chem. A. 126 (2022) 5940–5964. https://doi.org/10.1021/acs.jpca.2c01291.

[61] S.P. Bharadwaj, M.F. Modest, Medium resolution transmission measurements of CO_2 at high temperature-an update, J. Quant. Spectrosc. Radiat. Transf. 103 (2007) 146–155. https://doi.org/10.1016/j.jqsrt.2006.05.011.

[62] V. Evseev, A. Fateev, S. Clausen, High-resolution transmission measurements of CO_2 at high temperatures for industrial applications, J. Quant. Spectrosc. Radiat. Transf. 113 (2012) 2222–2233. https://doi.org/10.1016/j.jqsrt.2012.07.015.

[63] E.V. Karlovets, S. Kassi, S.A. Tashkun, V.I. Perevalov, A. Campargue, High sensitivity Cavity Ring Down spectroscopy of carbon dioxide in the 1.19–1.26μm region, J. Quant. Spectrosc. Radiat. Transf. 144 (2014) 137–153. https://doi.org/10.1016/j.jqsrt.2014.04.001.

[64] O.L. Polyansky, K. Bielska, M. Ghysels, L. Lodi, N.F. Zobov, J.T. Hodges, J. Tennyson, High-Accuracy CO_2 Line Intensities Determined from Theory and Experiment, Phys. Rev. Lett. 114 (2015) 243001. https://doi.org/10.1103/PhysRevLett.114.243001.

[65] J. Tennyson, S.N. Yurchenko, A.F. Al-Refaie, E.J. Barton, K.L. Chubb, P.A. Coles, S. Diamantopoulou, M.N. Gorman, C. Hill, A.Z. Lam, L. Lodi, L.K. McKemmish, Y. Na, A. Owens, O.L. Polyansky, T. Rivlin, C. Sousa-Silva, D.S. Underwood, A. Yachmenev, E. Zak, The ExoMol database: Molecular line lists for exoplanet and other hot atmospheres, J. Mol. Spectrosc. 327 (2016) 73–94. https://doi.org/10.1016/j.jms.2016.05.002.

[66] I.E. Gordon, L.S. Rothman, R.J. Hargreaves, R. Hashemi, E.V. Karlovets, F.M. Skinner, E.K. Conway, C. Hill, R.V. Kochanov, Y. Tan, P. Wcisło, A.A. Finenko, K. Nelson, P.F. Bernath, M. Birk, V. Boudon, A. Campargue, K.V. Chance, A. Coustenis, B.J. Drouin, J. –M. Flaud, R.R. Gamache, J.T. Hodges, D. Jacquemart, E.J. Mlawer, A.V. Nikitin, V.I. Perevalov, M. Rotger, J. Tennyson, G.C. Toon, H. Tran, V.G. Tyuterev, E.M. Adkins, A. Baker, A. Barbe, E. Canè, A.G. Császár, A. Dudaryonok, O. Egorov, A.J. Fleisher, H. Fleurbaey, A. Foltynowicz, T. Furtenbacher, J.J. Harrison, J. –M. Hartmann, V. –M. Horneman, X. Huang, T. Karman, J. Karns, S. Kassi, I. Kleiner, V. Kofman, F. Kwabia–Tchana, N.N. Lavrentieva, T.J. Lee, D.A. Long, A.A. Lukashevskaya, O.M. Lyulin, V.Y. Makhnev, W. Matt, S.T. Massie, M. Melosso, S.N. Mikhailenko, D. Mondelain, H.S.P. Müller, O.V. Naumenko, A. Perrin, O.L. Polyansky, E. Raddaoui, P.L. Raston, Z.D. Reed, M. Rey, C. Richard, R. Tóbiás, I. Sadiek, D.W. Schwenke, E. Starikova, K. Sung, F. Tamassia, S.A. Tashkun, J. Vander Auwera, I.A. Vasilenko, A.A. Vigasin, G.L. Villanueva, B. Vispoel, G. Wagner, A. Yachmenev, S.N. Yurchenko, The HITRAN2020 molecular spectroscopic database, J. Quant. Spectrosc. Radiat. Transf. 277 (2022) 107949. https://doi.org/10.1016/j.jqsrt.2021.107949.

[67] S.A. Tashkun, V.I. Perevalov, J.L. Teffo, L.S. Rothman, V.G. Tyuterev, Global fitting of $^{12}C^{16}O_2$ vibrational-rotational line positions using the effective Hamiltonian approach, J. Quant. Spectrosc. Radiat. Transf. 60 (1998) 785–801. https://doi.org/10.1016/S0022-4073(98)00082-X.

[68] D.A. Long, Z.D. Reed, A.J. Fleisher, J. Mendonca, S. Roche, J.T. Hodges, High-Accuracy Near-Infrared

Carbon Dioxide Intensity Measurements to Support Remote Sensing, Geophys. Res. Lett. 47 (2020). https://doi.org/10.1029/2019GL086344.

[69] H. Fleurbaey, H. Yi, E.M. Adkins, A.J. Fleisher, J.T. Hodges, Cavity ring-down spectroscopy of CO_2 near $\lambda = 2.06$ μm: Accurate transition intensities for the Orbiting Carbon Observatory-2 (OCO-2) "strong band," J. Quant. Spectrosc. Radiat. Transf. 252 (2020) 107104. https://doi.org/10.1016/j.jqsrt.2020.107104.

[70] M. Birk, C. Röske, G. Wagner, High accuracy CO_2 Fourier transform measurements in the range 6000–7000 cm^{-1}, J. Quant. Spectrosc. Radiat. Transf. 272 (2021) 107791. https://doi.org/10.1016/j.jqsrt.2021.107791.

[71] R.R. Gamache, C. Roller, E. Lopes, I.E. Gordon, L.S. Rothman, O.L. Polyansky, N.F. Zobov, A.A. Kyuberis, J. Tennyson, S.N. Yurchenko, A.G. Császár, T. Furtenbacher, X. Huang, D.W. Schwenke, T.J. Lee, B.J. Drouin, S.A. Tashkun, V.I. Perevalov, R. V. Kochanov, Total internal partition sums for 166 isotopologues of 51 molecules important in planetary atmospheres: Application to HITRAN2016 and beyond, J. Quant. Spectrosc. Radiat. Transf. 203 (2017) 70–87. https://doi.org/10.1016/j.jqsrt.2017.03.045.

[72] C.R. Mulvihill, E.L. Petersen, High-temperature argon broadening of CO_2 near 2190 cm^{-1} in a shock tube, Appl. Phys. B. 123 (2017) 255. https://doi.org/10.1007/s00340-017-6830-8.

[73] D.D. Lee, F.A. Bendana, A.P. Nair, D.I. Pineda, R.M. Spearrin, Line mixing and broadening of carbon dioxide by argon in the ν_3 bandhead near 4.2 μm at high temperatures and high pressures, J. Quant. Spectrosc. Radiat. Transf. 253 (2020) 107135. https://doi.org/10.1016/j.jqsrt.2020.107135.

[74] J. Buldyreva, M. Chrysos, Semiclassical modeling of infrared pressure-broadened linewidths: A comparative analysis in CO_2–Ar at various temperatures, J. Chem. Phys. 115 (2001) 7436–7441. https://doi.org/10.1063/1.1394941.

[75] F. Thibault, B. Calil, J. Buldyreva, M. Chrysos, J.-M. Hartmann, J.-P. Bouanich, Experimental and theoretical CO_2–Ar pressure-broadening cross sections and their temperature dependence, Phys. Chem. Chem. Phys. 3 (2001) 3924–3933. https://doi.org/10.1039/b103625b.

[76] M.S. Wooldridge, R.K. Hanson, C.T. Bowman, Argon broadening of the R(48), R(50) and R(52) lines of CO_2 in the (0001) ← (0000) band, J. Quant. Spectrosc. Radiat. Transf. 57 (1997) 425–434. https://doi.org/10.1016/S0022-4073(96)00074-X.

[77] S.N. Yurchenko, W. Thiel, P. Jensen, Theoretical ROVibrational Energies (TROVE): A robust numerical approach to the calculation of rovibrational energies for polyatomic molecules, J. Mol. Spectrosc. 245 (2007) 126–140. https://doi.org/10.1016/j.jms.2007.07.009.